



# Optimal utilization of interconnected RESs to microgrid: a hybrid AWO-ANFIS technique

S. Padhmanabhaiyappan<sup>1</sup> · R. Karthik<sup>1</sup> · K. Ayyar<sup>2</sup>

Published online: 29 November 2019  
© Springer-Verlag GmbH Germany, part of Springer Nature 2019

## Abstract

This dissertation proposes an elite converter for the optimal utilization of hybrid renewable energy sources in the microgrid-associated systems using hybrid technique. Microgrid (MG)-associated systems are photovoltaic, wind turbine and battery. The proposed elite converter is the high conversion ratio (HCR) DC–DC converter with a maximum power point tracking (MPPT) controller. The main advantage of the converter is to eliminate the problem of high switch voltage stress. The proposed hybrid technique is the joint execution of both the adaptive whale optimization algorithm (AWOA) and adaptive neuro-fuzzy interference system (ANFIS), and hence, it is named as AWO-ANFIS technique. Here, AWOA technique is utilized to establish the exact control signals based on the power variation between the source side (renewable energy sources and battery) and load side. ANFIS technique is utilized for error minimization by using the achieved dataset from AWOA technique. Here, the reference currents of the controller are managed in view of the MPPT for solar and wind energy. In the proposed technique, the objective function is defined by the system data subject to equality and inequality constraints. Finally, the proposed technique is executed in the MATLAB/Simulink working platform and the execution is compared with the existing techniques. To test the performance of the proposed method, different case studies are conducted such as variation of irradiance under constant wind speed, variation of PV power under constant irradiance and load variation under constant irradiance and wind speed. For all the cases, the response of current, voltage and power of all the sources is analyzed and compared with that of the existing techniques such as GA, PSO and WOA. The statistical analysis of the proposed technique is also analyzed. Likewise, the computation time using various trails such as 100, 250, 500 and 1000 is also analyzed. The comparison results affirm that the proposed technique has less computational time than the existing techniques. Moreover, the proposed method is cost-effective power production of MG and effective utilization of renewable energy source without wasting the available energy.

**Keywords** Renewable energy sources (HRES) · MG system · DC–DC converter · MPPT · Adaptive whale optimization algorithm (AWOA) · Adaptive neuro-fuzzy interference system (ANFIS)

---

Communicated by V. Loia.

✉ S. Padhmanabhaiyappan  
padmanbha0719@gmail.com

<sup>1</sup> Department of Electrical & Electronics Engineering, SRM Valliammai Engineering College, Kattankulathur, Tamil Nadu, India

<sup>2</sup> Department of Electronics and Instrumentation Engineering, SRM Valliammai Engineering College, Kattankulathur, Tamil Nadu, India

## 1 Introduction

In the future power supply, the power generation technologies will assume a vital part because of less reliance on fossil fuels of energy production and expanded worldwide public awareness (Amin et al. 2017; Fahmi et al. 2017a; Abualigah 2019). For the operation and management of the electricity grid, large number of renewable energy sources (RESs) and distributed generators require new strategies to enhance the power supply quality and reliability (Abualigah and Hanandeh 2015). Since availability of RESs is variable and unpredictable, energy storage device is utilized at the DC interface (Fahmi et al. 2017b; Rahim et al. 2016). In the greater part of the cases, both solar and wind

energy complement each other because of instantaneous fluctuation of solar irradiation and wind speed (Fahmi et al. 2018a). Energy management of HRES system using the artificial intelligence (AI) techniques such as neural network (NN), fuzzy logic (FL) and adaptive neuro-fuzzy interference system (ANFIS) achieves better outcomes (Olatomiwa et al. 2016). But the thermal and electrical demand of a building requirement is supplied by the hybrid structure (Bruni et al. 2016; Almada et al. 2016). During rapid changes of wind speed under wind turbulence the oscillation damping in DC link voltage is quick while dispatching the extracted power (Basir Khan et al. 2016; Wu et al. 2016; Fahmi et al. 2018b).

The presented optimization techniques provide good solution due to the good global search ability (Fahmi et al. 2018c). Uncertainly the global best value is varying as the stochastic variables in the optimization techniques (Fahmi et al. 2018d). Microcontroller-based power management system for an independent microgrid with PV module and the energy component is given in Fahmi et al. (2018e, 2019a) and Ambia et al. (2014). For power management in a microgrid, the impact of continuous variations in solar irradiance and wind speed which is joined with load power variations is accounted in Fahmi et al. (2019b). The inverter reactive power compensation for load variation is improper sag ride though the inverter voltage would not be conceivable (Fahmi et al. 2019c). The most utilized topologies are the parallel and series hybrid topologies (Amin and Fahmi 2019). In the series hybrid topology, some energy sources, in general some energy storage devices, are specifically associated with the common DC bus without DC–DC power converter (Abualigah et al. 2017, 2018a, b). In the parallel hybrid topology, all the energy sources are associated with the common DC bus through DC–DC power converters (Fahmi et al. 2017c).

In this research, a novel control scheme is introduced to the optimal utilization of interconnected RESs in the MG-connected system. The proposed system is the combined execution of AWO-ANFIS control scheme. Here, the optimal utilization of interconnected RESs and the switching loss reduction are the main goals of the DC–DC converter. Likewise, the importance of the AWOA in the proposed method is to generate the optimal gain dataset and obtain the exact gain parameter by using the ANFIS technique.

The difference between the proposed technique and the existing technique is explained below.

It is pertinent to note here that the GA, PSO and other evolutionary algorithms cannot be employed in realistic techniques on account of the nonlinear traits likes valve point effects, forbidden operating zones and piecewise quadratic cost function. Hence, it becomes all the more essential to fine-tune the optimization techniques in order

that they are competent to overwhelm these deficiencies and to successfully tackle the identical hassles. The most modern version of the upgraded metaheuristic algorithms is the adaptive whale optimization algorithm (AWOA), which mimics the hunting mechanism of humpback whales in nature. AWOA has been authenticated to consistently maintain a track record of superior quality performance in finding quick solutions to various optimization dilemmas in the literature. Here, the solution of the WOA is modified by using the crossover and the mutation operator. Here, the crossover is achieved between the two individuals, and in the mutation process, the individuals are mutated randomly based on the given fitness function. The highly significant trait of WOA is that the step size constant is competent to fine-tune the precision of the prey location, with the end result of considerably quickening solution procedure. Moreover, though AWOA is devoid of memory, it functions just as competently as the algorithms endowed with memory. An adaptive neuro-fuzzy inference system or adaptive network-based fuzzy inference system (ANFIS) is a kind of artificial neural network that is based on Takagi–Sugeno fuzzy inference system. Since it integrates both neural networks and fuzzy logic principles, it has potential to capture the benefits of both in a single framework. Its inference system corresponds to a set of fuzzy IF–THEN rules that have learning capability to approximate nonlinear functions. Hence, ANFIS is considered to be a universal estimator. It has uses in intelligent situational aware energy management system. Hence, AWO-ANFIS technique is suitable for optimal utilization of hybrid renewable energy sources (HRES) in the microgrid (MG)-associated systems.

The proposed technique is executed in the MATLAB/Simulink working platform, and the execution is compared with the existing techniques. To test the performance of the proposed method, different case studies are conducted such as variation of irradiance under constant wind speed, variation of PV power under constant irradiance and load variation under constant irradiance and wind speed. For all the cases, the response of current, voltage and power of all the sources is analyzed and compared with that of the existing techniques such as GA, PSO and WOA. The statistical analysis of the proposed technique is also analyzed. Likewise, the computation time using various trails such as 100, 250, 500 and 1000 is also analyzed. The comparison results affirm that the proposed technique has less computational time than the existing techniques. Moreover, the proposed method is cost-effective power production of MG and effective utilization of renewable energy source without wasting the available energy. The remaining section of this research is delineated as follows. Section 2 includes a brief review of the recent research work. Section 3 depicts the proposed methodology of the present work. Sections 4

and 5 consolidate the simulation analysis and the conclusion part.

## 2 Recent research works: a brief review

Various research works have already existed in the literature which depended on the power management scheme for renewable energy sources utilizing different methods and different perspectives. A portion of the works is reviewed here.

For the management of data centers (DCS), SDN-based energy management scheme in the RES was presented by Aujla and Kumar (2018). In addition, to deal with the irregularity of renewable energy, the authors likewise have introduced a charging–discharging scheme. To pull in the EVs, an energy trading and reward point scheme was planned in the energy management scheme. To effectively deal with the loads in a grid operated microgrid, a fuzzy logic controller was actualized by Angalaeswari et al. (2017). The author likewise has used the MPPT with a fuzzy logic controller (FLC) for a grid operated microgrid established by solar system and battery. Indragandhi et al. (2018) have represented to solve the energy management issues by using renewable resources ideally, keeping up the state of charge (SOC) in batteries. In their methodology, a power transfer between the AC/DC microgrids was kept up by the introduced system. The authors likewise have used the multi-objective particle swarm optimization (MOPSO) for the power management in AC/DC microgrid. Zhang et al. (2017) have investigated a sort of utility engineering microgrid structure for examining hybrid power system and control strategies. The authors likewise have designed the dispatch control and energy management scheme to facilitate power portion among assortment renewable energy generation.

For a hybrid generation system in view of solar energy and combined with the grid, a control design by means of passivity-based control integrated with an energy management technique was exhibited by Patrone and Feroldi (2017). The authors additionally have introduced a comprehensive nonlinear model for dissected the execution of the control methodology. Javaid et al. (2017) have outlined a home energy management (HEM) controller based on four heuristic algorithms: Moreover, a hybrid procedure additionally actualized which was genetic-based PSO (GBPSO). For optimal energy management of the microgrid, a joining particle swarm optimization (PSO) and primary-dual interior point (PDIP) strategy were introduced by Goroohi Sardou et al. (2018). Additionally, the authors likewise have utilized a bi-objective technique to distinguish the most pessimistic scenario probable 24-h

scenario with the severest consequences for the system security.

Amirtharaj et al. (2019) have introduced an efficient converter for the utilization of HRES using hybrid technique. The introduced hybrid technique was the combination of adaptive grasshopper optimization algorithm (AGOA) and the artificial neural network (ANN), and hence, it was said to be as AGONN technique. In the introduced system, AGOA develops the exact control signals based on the power variation in the source and load side. ANN predicts the optimal datasets. Jasmine Kaur et al. (2019) have invented an energy management system in a grid-connected multi-microgrid network for a deregulated framework of electricity market. The novelty was optimally utilizing the available renewable energy source and maximizes the benefits of the overall multi-microgrid framework. Roy et al. (2019) have explained an intelligent technique for EMS-based recurrent neural network (RNN) and ant lion optimizer (ALO). The demand response was found by RNN, and the economic dispatch issues were solved by ALO technique.

### 2.1 The motivation of the research work

The review of the research work demonstrates that the power management scheme for RES is an essential contributing factor in the power system. The use of renewable generators like photo voltaic (PV), wind, etc. provides power using conventional sources with less pollution, but their implementation in grid causes several complications like circulating current, voltage harmonics, reduction in storage life, overvoltage and overcurrent in transient, etc. Apart from that other challenges like active–reactive power sharing and current sharing, power management among renewable sources and high penetration of renewable energy are required to be focused to increase the handling and working capability of microgrid. In this manner, to repay drawbacks of individual resources, a backup power supply, for example, control and regulation strategies are indispensable and vital for optimal power management in a microgrid environment. Management of power is sternly required in microgrid system. Several methods to manage power have been devised. They are fuzzy logic controller (FLC), bacterial foraging optimization algorithm (BFOA), genetic algorithm (GA), binary particle swarm optimization (BPSO) and so on. Even if the above-mentioned techniques generate the required power, they have their own merits and demerits. Here, the FLC does not require broad system modeling, but rather the drawbacks like adjustment of FLC parameters and fuzzy rules under different traffic conditions. The GA displays particular weight fluctuates with the dispersion of fitness inside a population. The drawbacks in the GA is more complex, easy to fall into

premature convergence and depends on the initial population. The complexities of these algorithms are high because of the expanded number of required examples. To conquer these difficulties, advanced optimal control approaches are utilized. In the related works, few control techniques are displayed to solve the power management issue; the previously mentioned constraints have motivated to do this research work.

### 3 Modeling and simulation of interconnected RESs to MG with the proposed controller

The architecture model of the interconnected RES-based MG-connected system with a proposed controller is shown in Fig. 1. In the system model, the RES is the combination of the PV panel and wind turbine system and the model joins the battery storage device and DC–DC energy converters with the proposed AWOA controller and loads. At first, the electrical energy made from the RESs (PV and

wind) which began from nature which can be passed on especially from the MG. Here, the segments of the architecture are interconnected by the DC energy converter and compile the energy acquired by both PV and wind systems, while the energy is spilling out to the load and MG over an AC–DC converter. In the system, the PV system is just a number of PV panel in like way the wind turbine exists of a permanent magnet synchronous generator (PMSG) and a rectifier. In this manner, the battery is associated with a DC converter by a procedure for a DC–DC bidirectional converter.

In the present work, the converter of the system is overseen by the conventional MPPT controller. Here, there is a need of DC–DC converter for the battery to control the degree of discharging influence and to direct the supply of charging current to the battery. Toward the fulfillment of this assignment, the mathematical model and the configuration of MG-connected systems, such as source side and grid side, and the MPPT control design have been considered from Caisheng Wang and Nehrir (2008), and the

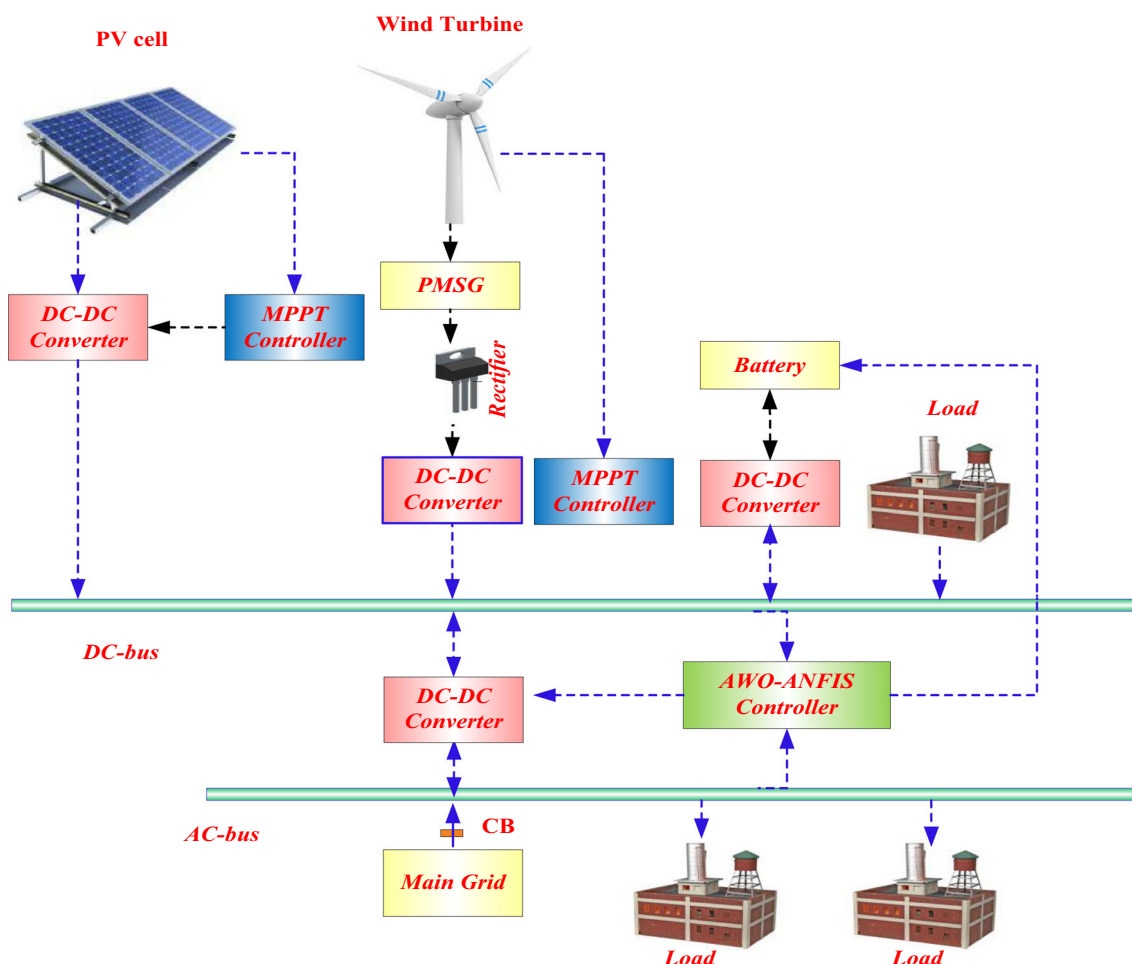


Fig. 1 Architecture of MG-connected system-based HRES with the proposed AWO-ANFIS controller

proposed converter and the controller configuration are explained in the accompanying section.

### 3.1 Design and modeling of the proposed HCR DC–DC converter

In the interconnected RES-based MG system, most of the time, the power deficiency is caused by using the PV and wind system based on the variable sunlight and atmosphere condition. For taking care of this circumstance, the majority of the mechanical businesses utilized the traditional converters such as buck, boost and buck–boost for tracking the maximum power. Nonetheless, these converters are not exceptional to track most extraordinary power in alterable atmosphere conditions.

To overcome these issues, the proposed method employed the integrated high conversion ratio (HCR) DC–DC converter with an MPPT controller. In this research, the role of the proposed HCR DC–DC converter is the disposal of high switch voltage stress and the integration of the converter effectiveness. The contribution of the converters is sourced by PV panels, and the output of the converters is associated with a resistive load. The proposed converter is the integrated model of the series-capacitor (SC) HCR DC–DC converter (Kim et al. 2018). The operation of the proposed converter is similar to the existing SC HCR DC–DC converter. But, the overall size of the components in the proposed converter is lower than that of the SC HCR DC–DC converter. The integrated

circuit model of the proposed DC–DC converter is obviously shown in Fig. 2.

Owing to the series connection of  $C_1$  and  $C_2$ ,  $V_{C_2}$  becomes  $V_{in} - V_{C_1}$ . Moreover,  $C_1$  and  $C_2$  are connected in parallel with  $V_{in}$ . Consequently, before the start-up, the capacitors are charged, and also, during the start-up, the switch voltages do not increase. Although, when compared with the existing SC HCR converter, the proposed converter has one more capacitor  $C_4$ , the size of the overall components is lower in the proposed converter. So, the proposed converter generates efficient results than the existing technique. The key waveform of the proposed converter is shown in Fig. 3, and the detailed operation modes are illustrated in Fig. 4. The proposed converter has three operation modes similar to the existing SC HCR converter. The operating principle of the proposed DC–DC converter is delineated in the section follows.

#### 3.1.1 Operating principle of the proposed converter

The operating principle of the proposed HCR DC–DC converter has three modes of operation. The obvious operations of three modes are depicted as follows.

(a) *Mode I* In this mode, the switch  $S_1$  is turned on and the diode  $D_2$  is conducted, whereas the diode  $D_1$  is not conducted which is shown in Fig. 3a. The switched inductance  $\delta_1$  ( $L_{S_1}, L_{S_2}, D_{S_1}, D_{S_2}, D_{S_3}$ ) is charged through  $S_1$ , whereas the current of switched inductance  $\delta_2$  ( $L_{S_3}, L_{S_4}, D_{S_4}, D_{S_5}, D_{S_6}$ ) freewheels through the diode  $D_2$ .

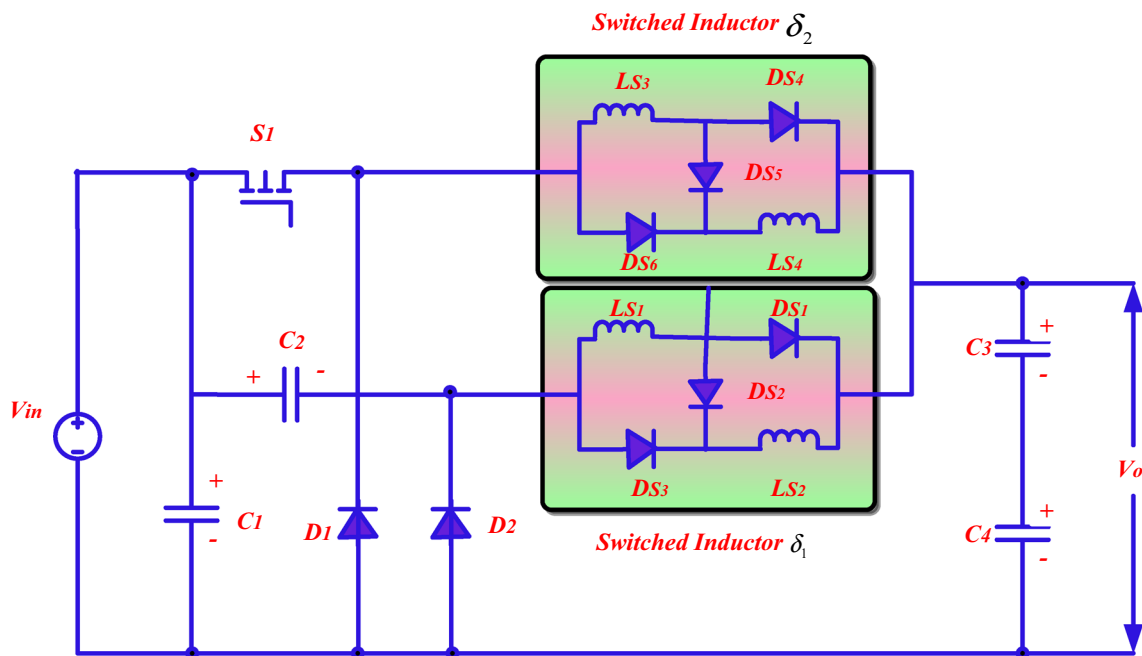
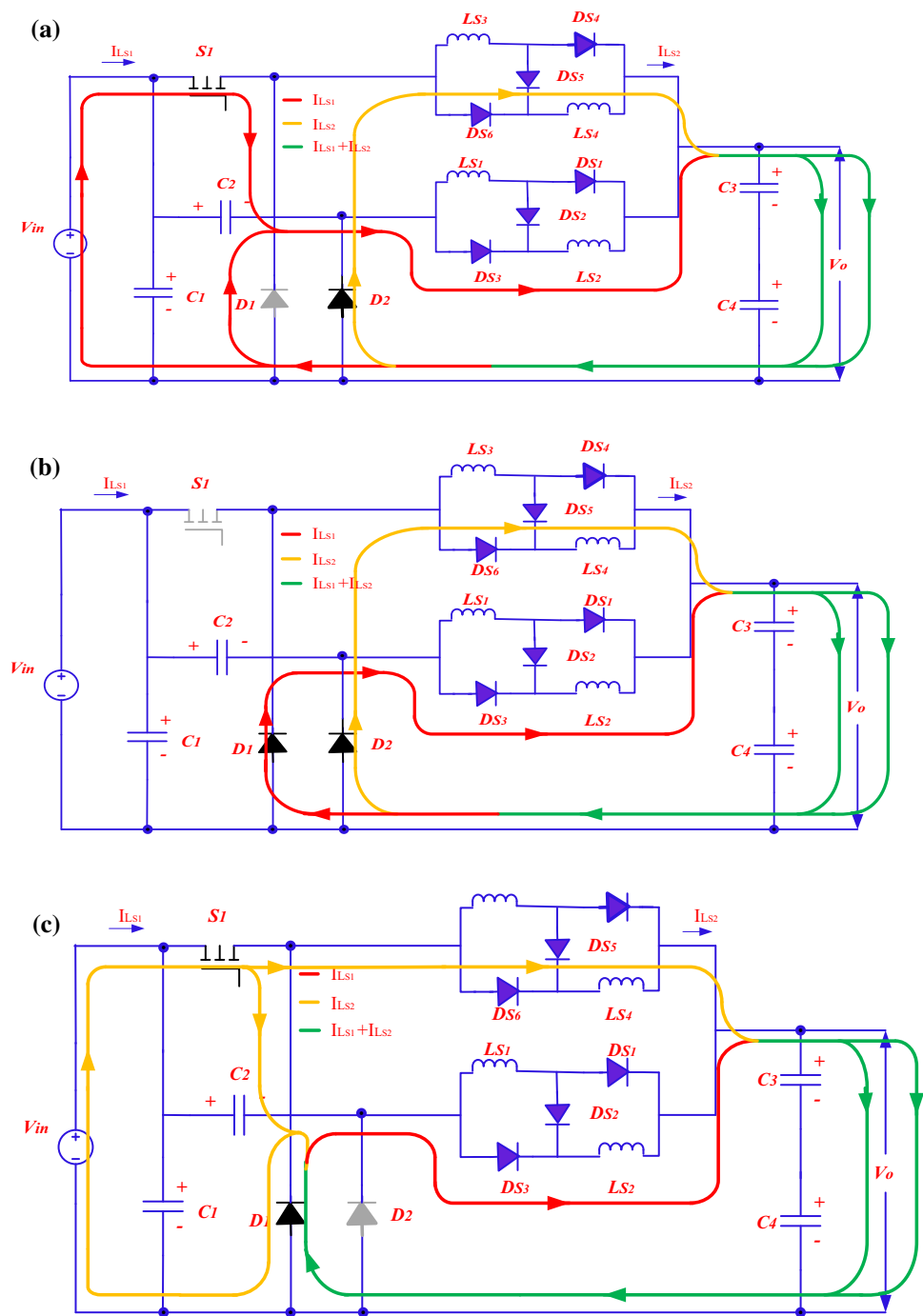


Fig. 2 Circuit diagram of an integrated HCR DC–DC converter

**Fig. 3** Modes of operation of the proposed converter: **a** Mode I, **b** Mode II, **c** Mode III



Owing to  $I_{\delta_1}$ ,  $C_1$  and  $C_2$  are charged and discharged, respectively.

(b) *Mode II* In this mode,  $D_1$  and  $D_2$  are conducted, whereas  $S_1$  is turned off which is shown in Fig. 3b. The two inductor currents ( $I_{\delta_1}$  and  $I_{\delta_2}$ ) freewheel through the diodes  $D_1$  and  $D_2$ , and there is no current flow in  $C_1$  and  $C_2$ .

(c) *Mode III* In mode 3,  $D_1$  is conducted, whereas  $S_1$  is turned off and  $D_2$  is not conducted which is shown in Fig. 3c. The inductor current  $I_{\delta_1}$  continues freewheeling

through the diode  $D_1$  and  $\delta_2$  is discharged, respectively. In this mode, the sum of the two inductor currents (or output current) flows through the diode.

The proposed converter has an efficient voltage gain than the existing SC HCR converter. Furthermore, owing to the charge balance condition of the capacitors  $C_1$  and  $C_2$ , the proposed converter retains the intrinsic inductor current balancing feature of the SC HCR converter; thus, the two inductor currents share the output current  $I_o$ .



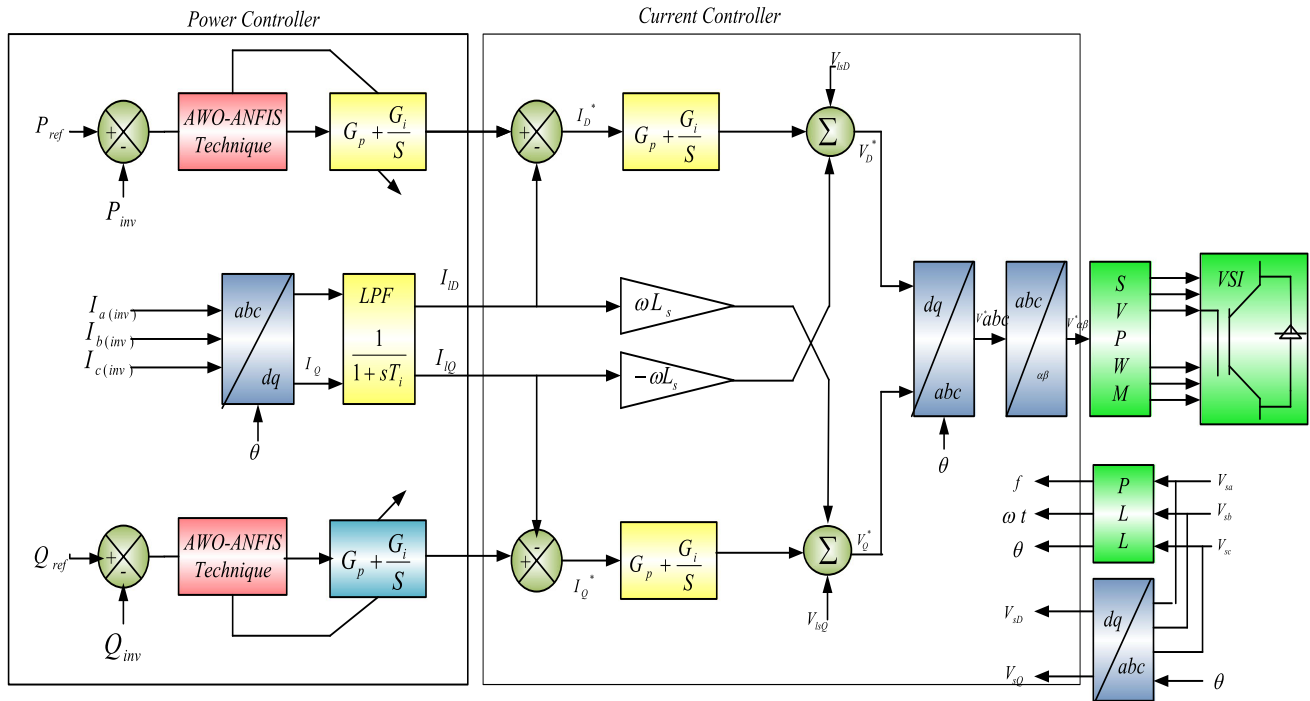


Fig. 4 Proposed controller scheme of HCR DC–DC converter

3.1.2 The control structure of the proposed HCR DC–DC converter

This section describes the proposed control structure of the DC–DC converter for the optimal utilization of the interconnected resources. The control structure of the DC–DC converter involves main blocks named as a power controller and a linear current controller which are utilized for real-time self-tuning of the power control parameters.

(a) Power control strategy

In this section, the power stream between the microgrid and the utility to the extent of providing controlled active and reactive power to the load is controlled by utilizing this procedure. As per Fig. 4, the two PI controller-based proposed power controllers are portrayed in the left section of the figure. Here, the external control loop is represented by the proposed controller, whereas the reference current vectors  $I_D^*$  and  $I_Q^*$  are produced through these employed control loop. In this paper, the AWO-ANFIS control strategy is presented for the ideal use of the interconnected RES-based MG unit; the active and reactive power are the main control objectives which must be achieved at the load change condition. In this mode, the active and reactive power output of the inverter is balanced by the controller based on its reference values of  $p_{ref}$  and  $\beta_{ref}$ ; besides with a specific end goal to discharge qualified reference current vectors, the optimal control parameters are given by the AWO-ANFIS control scheme. The reference current

vectors are communicated based on the  $DQ$  reference frame, and the PI regulators are expressed as follows,

$$I_D^* = (p_{ref} - p_{inv}) (G_{pp} + G_{ip}/s) \tag{1}$$

$$I_Q^* = (\beta_{ref} - \beta_{inv}) (G_{pQ} + G_{iQ}/s) \tag{2}$$

(b) Current control strategy

In this section, the precise tracking and short drifters of the inverter output current are guaranteed by the controller. As per Fig. 4, a synchronous reference frame-based current control loop configuration is delineated in the right section of the figure. This controller is typically used so that the voltage is applied to the inductive  $R - L$  impedance so a drive current in the inductor has a minimum error. Here, the voltage phase angle in the control scheme is identified by the phase-locked loop (PLL) block, and furthermore, the current error is disposed through the two PI regulators. Also, the steady-state and dynamic performance of the system is enhanced by the inverter current loop and the grid voltage feed-forward loop. Therefore, the reference voltage signals in the  $DQ$  frame are represented by the output signals of the controller. The reference voltage signals in the synchronous  $DQ$  frame can be expressed as follows,

$$\begin{bmatrix} V_D^* \\ V_Q^* \end{bmatrix} = \begin{bmatrix} -(G_p \cdot I_D + \omega L_s \cdot I_Q) \\ \omega L_s \cdot I_D - G_x \cdot I_Q \end{bmatrix} + \begin{bmatrix} G_p \cdot I_D^* \\ G_p \cdot I_Q^* \end{bmatrix} + \begin{bmatrix} G_i \cdot \delta_D \\ G_i \cdot \delta_Q \end{bmatrix} + \begin{bmatrix} V_{sD} \\ V_{sQ} \end{bmatrix} \tag{3}$$

$$\frac{d\delta_D}{dt} = I_D^* - I_D \quad \frac{d\delta_Q}{dt} = I_Q^* - I_D \tag{4}$$

The above equation can be transformed into  $xy$  the stationary frame by using Clarke’s transformation which is expressed as follows,

$$\begin{bmatrix} V_x \\ V_y \\ V_0 \end{bmatrix} = \frac{2}{3} \begin{bmatrix} V_x \\ V_y \\ V_z \end{bmatrix} \begin{bmatrix} 1 & -0.5 & -0.5 \\ 0 & 0.866 & -0.866 \\ 0.5 & 0.5 & 0.5 \end{bmatrix} \tag{5}$$

Furthermore, by using the low-pass filter (LPF) the inductor current is computed. In this work, the LPF is presented as a first-order transfer function which is given by:

$$F \frac{1}{1 + sT_i} = F_l \tag{6}$$

where the output value of the filter is expressed as  $F$ , the filtered value is represented as  $F_l$  and the constant time is denoted as  $T_i$ .

### 3.2 Optimal utilization of interconnected RESs using AWO-ANFIS control scheme

This section presented the novel scheme for the optimal utilization of interconnected RESs in the MG system. For the optimal utilization, the proposed work is the combined execution of the adaptive whale optimization algorithm (AWOA) and adaptive neuro-fuzzy interference system (ANFIS). Here, the optimal dataset of the control signal for the offline way is generated by the AWOA algorithm based on the power variation between the source side and the load side. Here, the reference currents of the controller are managed based on the maximum power point tracking (MPPT) of the proposed hybrid control technique for solar and wind energy. The optimal signal for the online way is predicted through the ANFIS technique, and also, the control procedure is performed by ANFIS technique in less execution time. The description of the proposed technique is illustrated in the following section.

#### 3.2.1 Optimal dataset generation using AWOA

The AWOA is one of the recent metaheuristic algorithms used for solving the optimization problems. This algorithm was presented by Mirjalili and Lewis Mirjalili and Lewis (2016). In this algorithm, the whales are the exceptionally wise creatures with movement. It is the remarkable chasing

conduct of the humpback whales. Generally, the humpback whales chase the little fishes from the surface of the ocean. In this algorithm, the humpback whales used the bubble-net feeding strategy for one of the kinds of chasing processes. Here, the whales make an unmistakable bubble along nine molded ways by swimming around the prey. The scientific assessment of AWOA is assessed in view of encircling prey, bubble-net hunting method and search prey. In the proposed strategy, the optimization procedure starts by creating a random population of whales.

#### Step (i): Exploitation Phase (Encircling Prey)

In this initialization step, the input proportional and integral gain parameters such as  $G_p$  and  $G_i$  are randomly generated which are given as follows,

$$X_i = \begin{bmatrix} G_p^{11} G_i^{11} & G_p^{12} G_i^{12} & \dots & G_p^{1n} G_i^{1n} \\ G_p^{21} G_i^{21} & G_p^{22} G_i^{22} & \dots & G_p^{2n} G_i^{2n} \\ \vdots & \vdots & \vdots & \vdots \\ G_p^{m1} G_i^{m1} & G_p^{m2} G_i^{m2} & \dots & G_p^{mn} G_i^{mn} \end{bmatrix} \tag{7}$$

where  $G_p$  and  $G_i$  are the gain parameters.

#### Step (ii) Bubble-Net Hunting Method

There are two approaches are involved in the bubble-net hunting method. They are: (1) shrinking encircling prey and (2) spiral position updating (Aljarah et al. 2016).

##### (a) Shrinking encircling prey

The fitness of the population is evaluated by using the position of the shrinking encircling prey (Oliva et al. 2017). The required objective function is given in the following equation,

$$J = \text{Min}\{E\} \tag{8}$$

where  $J$  is the objective function value which is added with the actual objective function,  $t$  is the time and  $E$  is the error signal.

##### (b) Spiral position updating

After the fitness calculation of each individual, the best optimal solution is updated according to the value of  $J$ . After the updating process, the target solution  $T_A$  is updated if any better solution is found, i.e.,  $i = i + 1$ .

#### Step (iii) Prey Search

Here, the solution of the WOA is modified by using the crossover and the mutation operator (Abualigah and Khader 2017). Here, the crossover is achieved between the two individuals, and in the mutation process, the individuals are mutated randomly based on the given fitness function. The crossover and mutation are computed as follows (Mafarja and Mirjalili 2017; Kaveh and Ghazaan 2016),



$$\text{Crossover} = \frac{\gamma_{Gc}}{L_c} \tag{9}$$

$$\text{Mutation} = \frac{\lambda_{pt}}{L_c} \tag{10}$$

where  $\gamma_{Gc}$  is the number of gene crossover and  $L_c$  is the length of the individuals,  $\lambda_{pt}$  is the mutation point and  $L_c$  is the length of the individual. Using the updated movement, find the fitness and check the objective function.

*Step (iv): Termination*

Check the stopping criterion. If it is not satisfied, go to step 3; else, terminate the search. Finally, the updated optimal solutions are given as follows,

$$\begin{bmatrix} E^{11} & E^{12} & \dots & E^{1n} \\ E^{21} & E^{22} & \dots & E^{2n} \\ \vdots & \vdots & \vdots & \vdots \\ E^{m1} & E^{m2} & \dots & E^{mn} \end{bmatrix} = \begin{bmatrix} G_p^{11}G_i^{11} & G_p^{12}G_i^{12} & \dots & G_p^{1n}G_i^{1n} \\ G_p^{21}G_i^{21} & G_p^{22}G_i^{22} & \dots & G_p^{2n}G_i^{2n} \\ \vdots & \vdots & \vdots & \vdots \\ G_p^{m1}G_i^{m1} & G_p^{m2}G_i^{m2} & \dots & G_p^{mn}G_i^{mn} \end{bmatrix} \tag{11}$$

Once the above steps of the algorithm are completed, the system is able to select the optimal utilization of HRES based on the optimal gain parameters and the limited error.

**3.2.2 Control pulse generation using ANFIS**

The ANFIS is one of the AI techniques which combine both the fuzzy logic and the artificial neural networks. The adaptive NF interference system is illustrated in Fig. 5. The ANFIS technique consists of five phases (Selvara 2017). They are rule base, database, a decision-making unit, a fuzzification interface and a defuzzification interface. Here, five network layers are used to generating these five phases.

*Layer 1* Layer 1 consists of a number of nodes whose activation functions are triangular functions.

*Layer 2* The minimum values of the inputs are selected by this layer.

*Layer 3* Each input is normalized by this layer with respect to the others.

*Layer 4* In this layer, the output of *i*th node is a linear function of the output of *i*th node generated from the third layer and the ANFIS input signals.

*Layer 5* All the incoming signals are summed up by this layer. Based on the least square error estimation and the backpropagation algorithm, the ANFIS structure can be automatically tuned.

In the proposed approach, the previously detected gain parameters are given as input of the ANFIS. The output of the ANFIS is the optimal control pulse. Based on these corresponding inputs and the output values, the ANFIS is

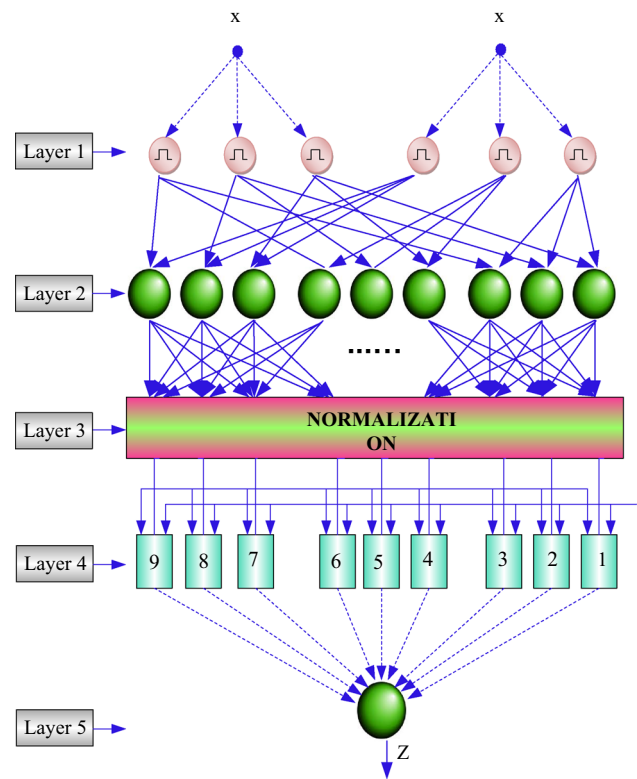


Fig. 5 Structure of the ANFIS

trained (Nürnberger et al. 1999). The structure and the training process of the ANFIS are depicted as follows.

**3.2.2.1 A proposed structure of ANFIS** *First Layer* In the first layer of ANFIS, the gain parameters  $G_p$  and  $G_i$  are multiplied by corresponding weights such as  $W_{yz}^3, W_y^2$  and  $W_{ab}^2$  of ANFIS which are mapped through a fuzzy logic membership functions. For every parameter, the fuzzy logic functions are chosen to be triangle-shaped.

*Second Layer* By determining the firing strengths of the rules, a minimum error value of three input weights is computed in the second layer which is given as follows,

$$W_i = \min(W_{bc}^3(SE), W_b^2(I_Q), W_{ab}^2(I_Q^*)) \tag{12}$$

*Third Layer* The normalization process of the weight values are computed in the third layer. The ratio between the strength of the *k*th rule and sum of the firing strengths is known as the normalized value of the firing strengths, which are expressed as follows (Yadegaridehkordi et al. 2018),

$$\bar{W}_i = \frac{W_i}{\sum W_i} \tag{13}$$

*Fourth Layer* The defuzzification adaptive nodes are computed in the fourth layer. The output of the fourth layer is computed as follows,

$$\bar{W}_k = \alpha_i x + \beta_i y + (-\chi_i z) + r_i \quad (14)$$

The output of the fourth layer can be defined as follows,

$$Y_4 = \bar{W}_i f_i = \bar{W}_i (\alpha_i x + \beta_i y + (-\chi_i z) + r_i) \quad (15)$$

where  $\alpha = \beta = \chi = 0$ , so the output of layer 4 can be rewritten as,

$$Y_4 = \bar{W}_i f_i = \bar{W}_i (r_i) \quad (16)$$

*Fifth Layer* The weighted output of the consequent parameter's summation value is the output of the fifth layer and it is expressed as follows,

$$Y_5 = \sum_i \bar{W}_i f_i = \frac{\sum_i \bar{W}_i f_i}{\sum_i \bar{W}_i} \quad (17)$$

Finally, the ANFIS generate the beneficial control pulses and the corresponding parameter for those pulses after completing the algorithm. The structure of the proposed hybrid technique is depicted in Fig. 6.

## 4 Simulation results and discussions

In this section, the simulation evaluation of the optimal utilization of interconnected renewable energy resources with the proposed AWO-ANFIS control technique is

described. Here, the optimal generation of the control signal is handled by the AWO-ANFIS controller; after that, the signal is exchanged to both MPPT controllers of PV and wind generating system and also for the proposed converter. Based on the PV, wind and battery converter output, the performance of the proposed is evaluated. Here, the performance of the proposed AWO-ANFIS technique is compared with that of the existing techniques such as genetic algorithm (GA) (Duan et al. 2015; Mohamed Imran and Kowsalya 2014), particle swarm optimization algorithm (PSO) (Prince et al. 2018; Rezaee Jordehi et al. 2015) and the whale optimization algorithm (WOA) (Sahu et al. 2018). Moreover, the performance of the proposed method is tested in the MATLAB/Simulink working platform by using different case studies.

### Case 1: Variation of irradiance under constant Wind Speed

Case study 1 illustrates the variation of irradiance under constant wind speed which is clearly illustrated in Fig. 7. Here, Fig. 7a illustrates the variation of irradiance and Fig. 7b shows the constant wind speed. Gain from this figure, the irradiance and the wind speed are plotted between the time intervals of 0 s and 1 s. In those figures,

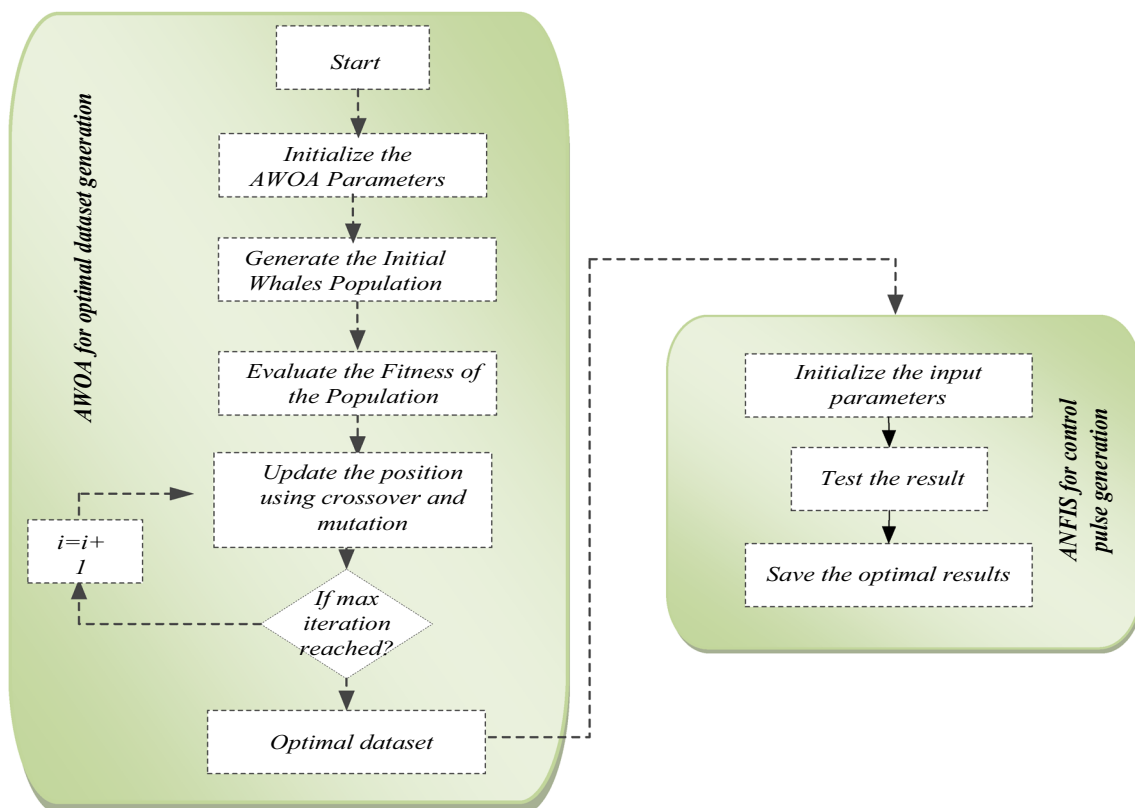


Fig. 6 Flowchart of the proposed AWO-ANFIS technique

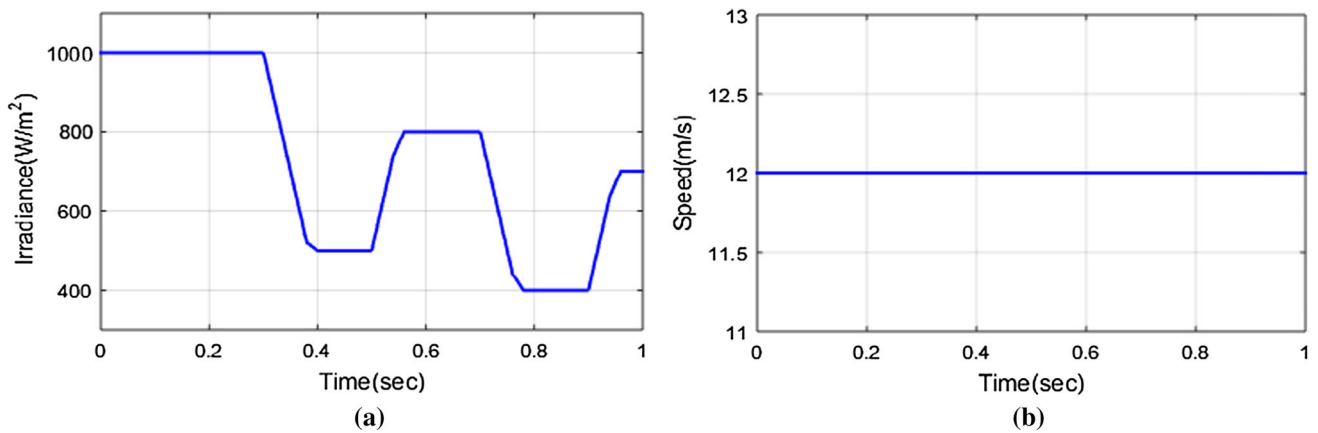


Fig. 7 Variation of irradiance under constant wind speed: **a** Irradiance. **b** Wind speed

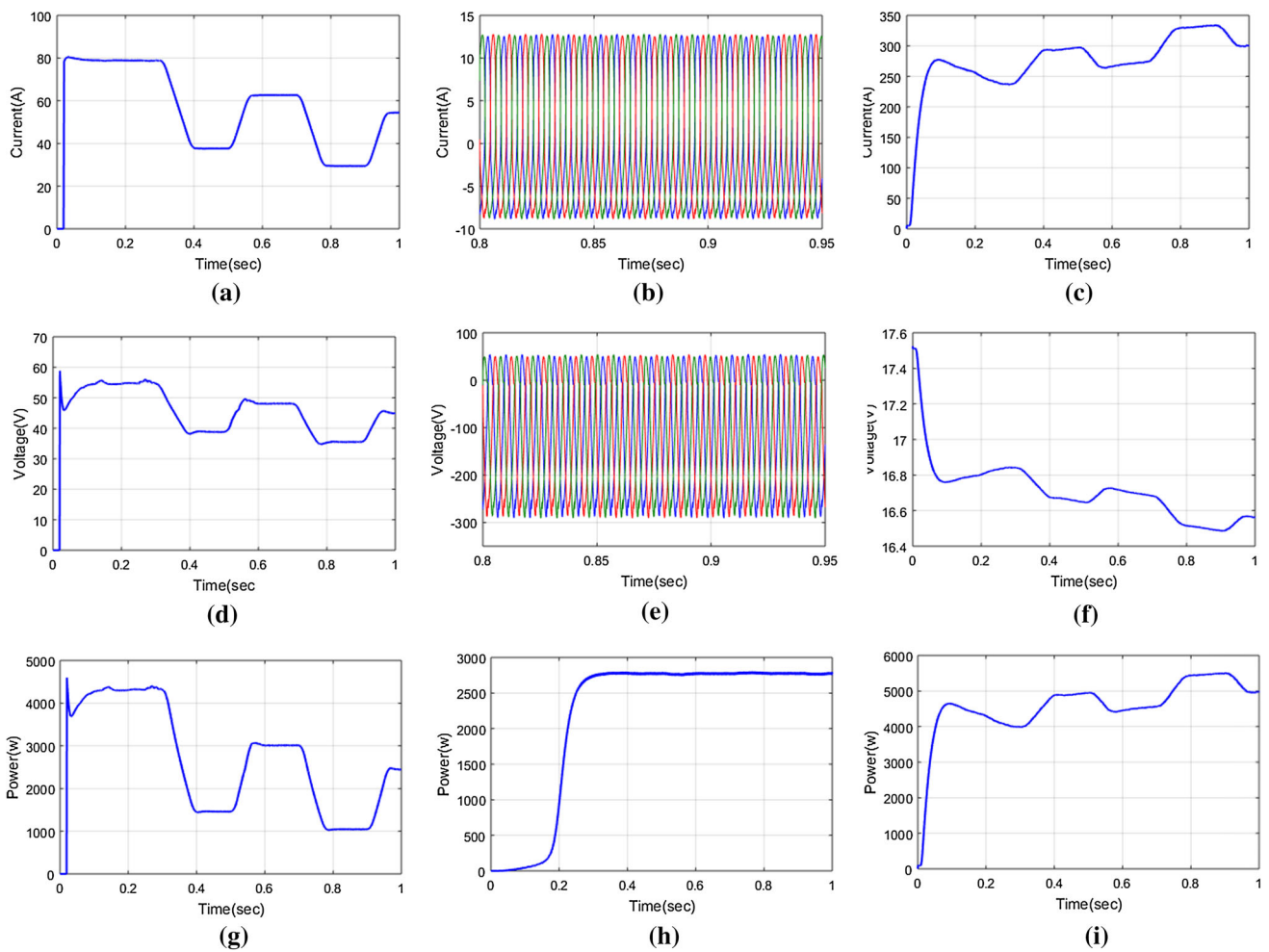


Fig. 8 Performance of PV power under variation of irradiance: **a** PV current, **b** wind current, **c** battery current, **d** PV voltage, **e** wind voltage, **f** battery voltage, **g** PV power, **h** wind power and **i** battery power

by varying irradiance under constant wind speed the performance of the proposed technique is evaluated.

Figure 8 illustrates the current, voltage and power of the proposed PV, wind and the battery system under constant

wind speed. Here, Fig. 8a shows the PV current which has been plotted between the time intervals of 0 and 1 s. Here, the PV current is varied between the time intervals of 0.1 and 1 s. The current signal of the wind is illustrated in

Fig. 7b and this signal is plotted between the time intervals of 0 and 0.28 s; after that, it remains constant. The current signal of the battery is illustrated in Fig. 8c, and in that plot, the curve reaches the maximum value of 330 A, and till the end of the operation, the signal is slightly reduced and reaches the 300 A.

Likewise, Fig. 8d illustrates the PV voltage which has been plotted between the time intervals 0 and 1 s. The generated voltage signal of the PV is varied between the time intervals of 0.1 and 1 s. The voltage signal of the wind is illustrated in Fig. 8e, and this signal is plotted between the time intervals of 0 and 0.29 s. The voltage signal of the battery is illustrated in Fig. 8f, and in that plot, the curve reaches the maximum value of 17.5 V, and till the end of the operation, the signal is slightly reduced and reaches the 16.59 V.

Similarly, Fig. 8g illustrates the PV power which is also plotted between the time intervals 0 and 1 s. The generated voltage signal of the PV is varied between the time intervals of 0.1 and 1 s; before that, it was constant. The power

signal of the wind is illustrated in Fig. 8h, and this signal is plotted between the time intervals of 0 and 1 s. The power signal of the battery is illustrated in Fig. 8i, and in that plot, the curve reaches the maximum value of 5500 W, and till the end of the operation, the signal is slightly reduced and reaches the 5000 W.

The performance of the dynamic response of the current, voltage and power of the grid, load and inverter is illustrated in Fig. 9. Here, the currents of the grid, load and inverter are illustrated in Fig. 9a–c; these three plots are varied between the time intervals of 0.1 and 1 s. The maximum values of the current in the grid and load are 3A, 200A and 400A, respectively. The voltage signals of the grid, load and inverter are illustrated in Fig. 9d–f; these three voltage signals are varied between the time intervals of 0.1 and 1 s. The maximum values of the voltage in the grid and load are 750 V, 750 V and 10 V, respectively. The power signals of the grid, load and inverter are illustrated in Fig. 9g–i; these three power signals are varied between the time intervals of 0 and 1 s. The maximum

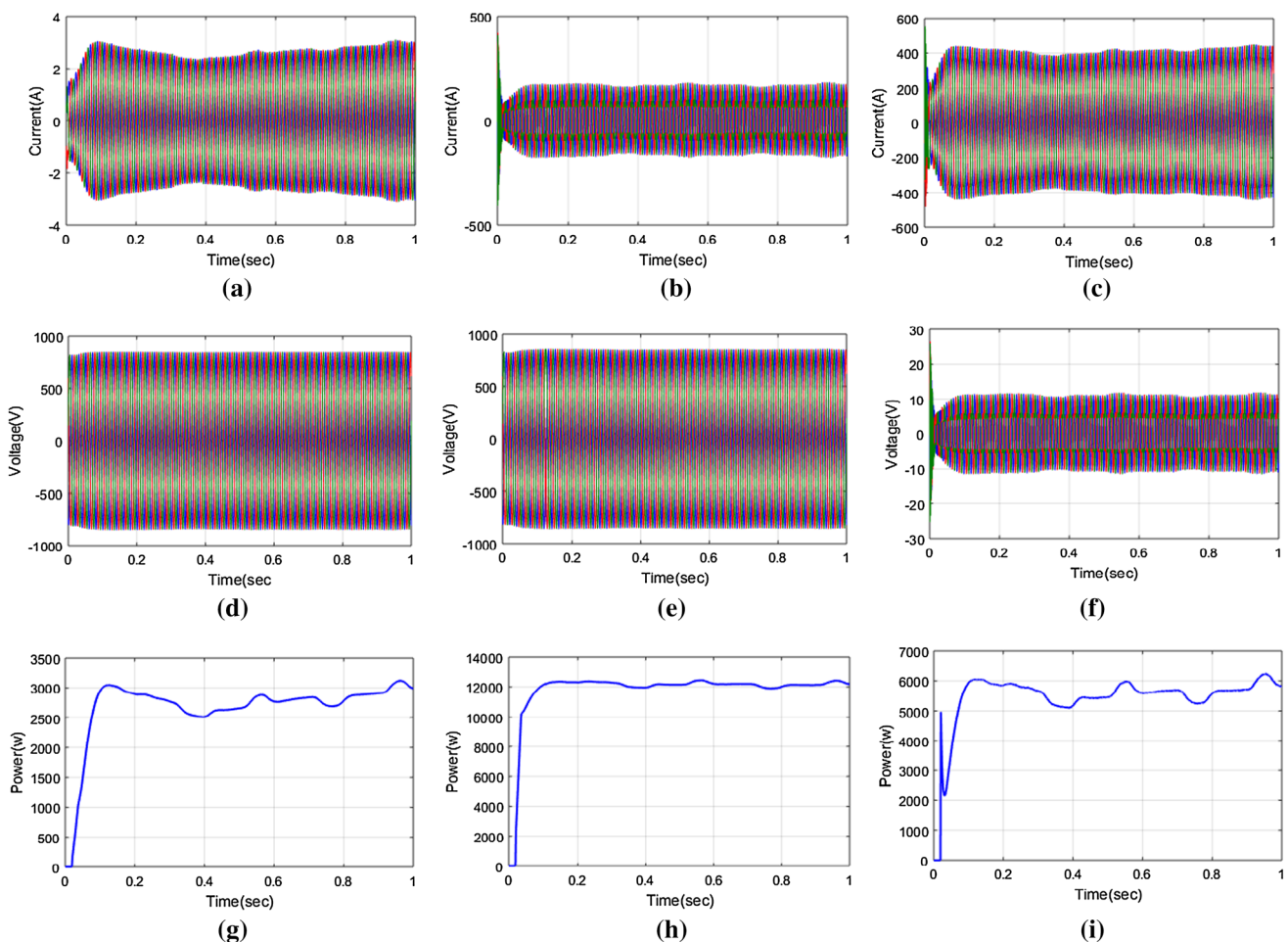


**Fig. 9** Performance of the proposed technique under constant wind speed: **a** grid current, **b** load current, **c** inverter current, **d** grid voltage, **e** load voltage, **f** inverter voltage **g** grid power, **h** load power and **i** inverter power

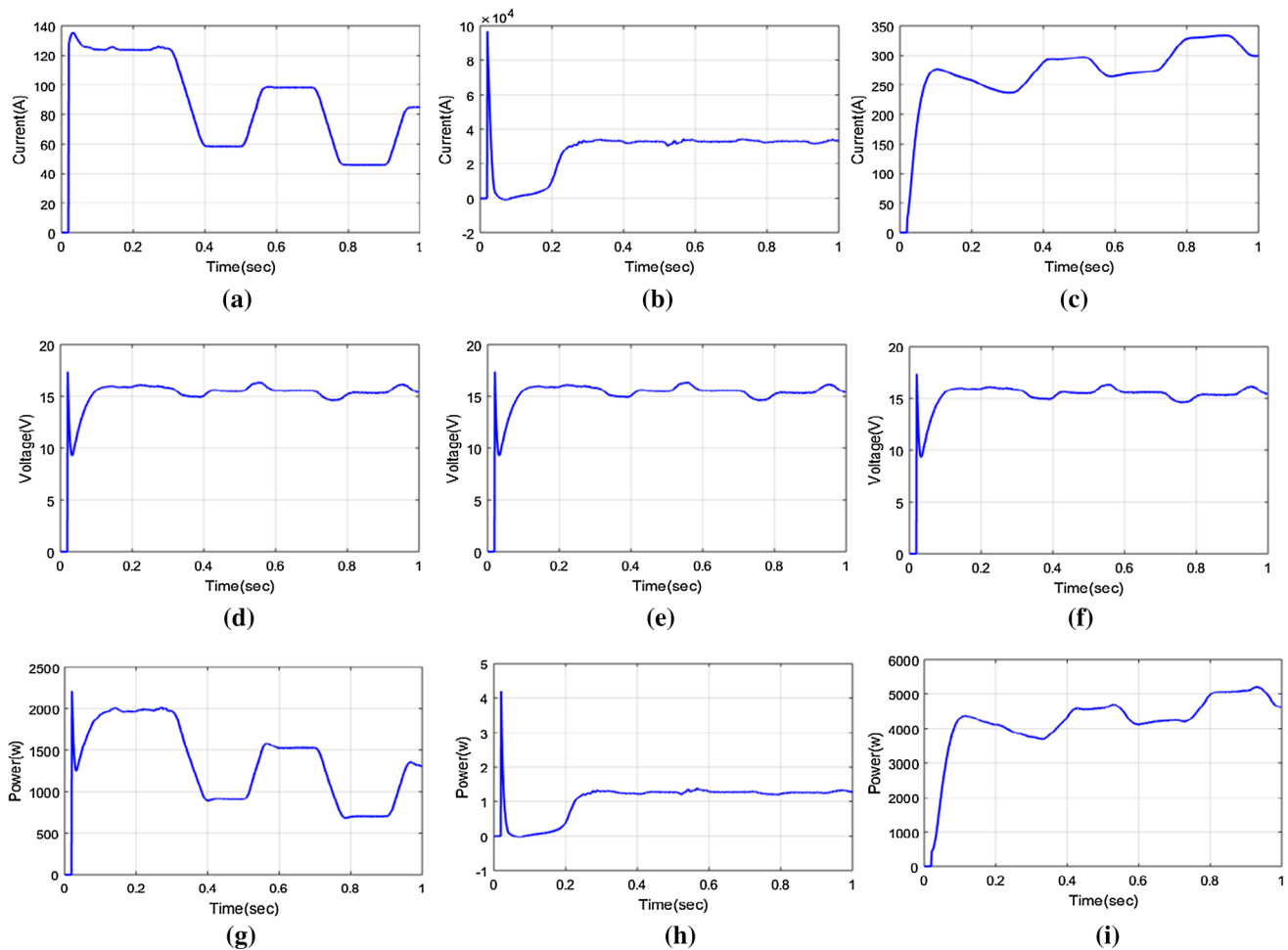


**Fig. 10** Performance of the converter using AWO-ANFIS: **a** PV current, **b** wind current, **c** battery current, **d** PV voltage, **e** wind voltage, **f** battery voltage, **g** PV power, **h** wind power and **i** battery power

values of the power in the grid, load and inverter are 3000 W, 12000 W and 6000 W, respectively.

Figure 10 shows the performance of the current, voltage and power of the PV, wind and battery by using the AWO-ANFIS control scheme. The current signals of the PV, wind and battery are delineated in Fig. 10a–c. In these three plots, the signal is plotted between the instants of 0 and 1 s. The maximum values of the current in the PV, wind and battery are 138 A,  $9.99 \times 10^4$  A and 340 A, respectively. Likewise, the voltage signals of the PV, wind and battery are delineated in Fig. 10d–f. In these three plots, the signal is plotted between the instants of 0 and 1 s. The maximum values of the voltage in the PV, wind and battery are 17.5 V, 17 V and 18 V, respectively. Similarly, the power signals of the PV, wind and battery are delineated in Fig. 10g–i. In these three plots, the signal is plotted between the instants of 0 and 1 s. The maximum values of the current in the PV, wind and battery are 2300 W, 6 W and 5100 W, respectively.

The power comparison of the PV, wind, battery and load is clearly depicted in Fig. 11. Here, the power of the proposed technique is maintained by using AWO-ANFIS control scheme, and also, the performance of the proposed method is compared with that of the GA, PSO and WOA (Aljarah et al. 2016) approach. The individual power of PV is illustrated in Fig. 11a; here, the proposed AWO-ANFIS approach has high power when compared with the existing methods during the time intervals of 0.56 to 0.6 s.

The maximum power value of the proposed scheme is 1580 W. In the remaining instants, the power value of all the techniques is similar. The individual power of wind is illustrated in Fig. 11b; here, the proposed AWO-ANFIS approach has high power during the time intervals of 0.56 to 0.6 s. The maximum power value of the proposed scheme is 275 W. The individual power of the battery is illustrated in Fig. 11c; here, the proposed AWO-ANFIS approach has high power during the time intervals of 0.8 to 1 s; here, the maximum power value in the battery is 5300 W. The power of the load is illustrated in Fig. 11d.



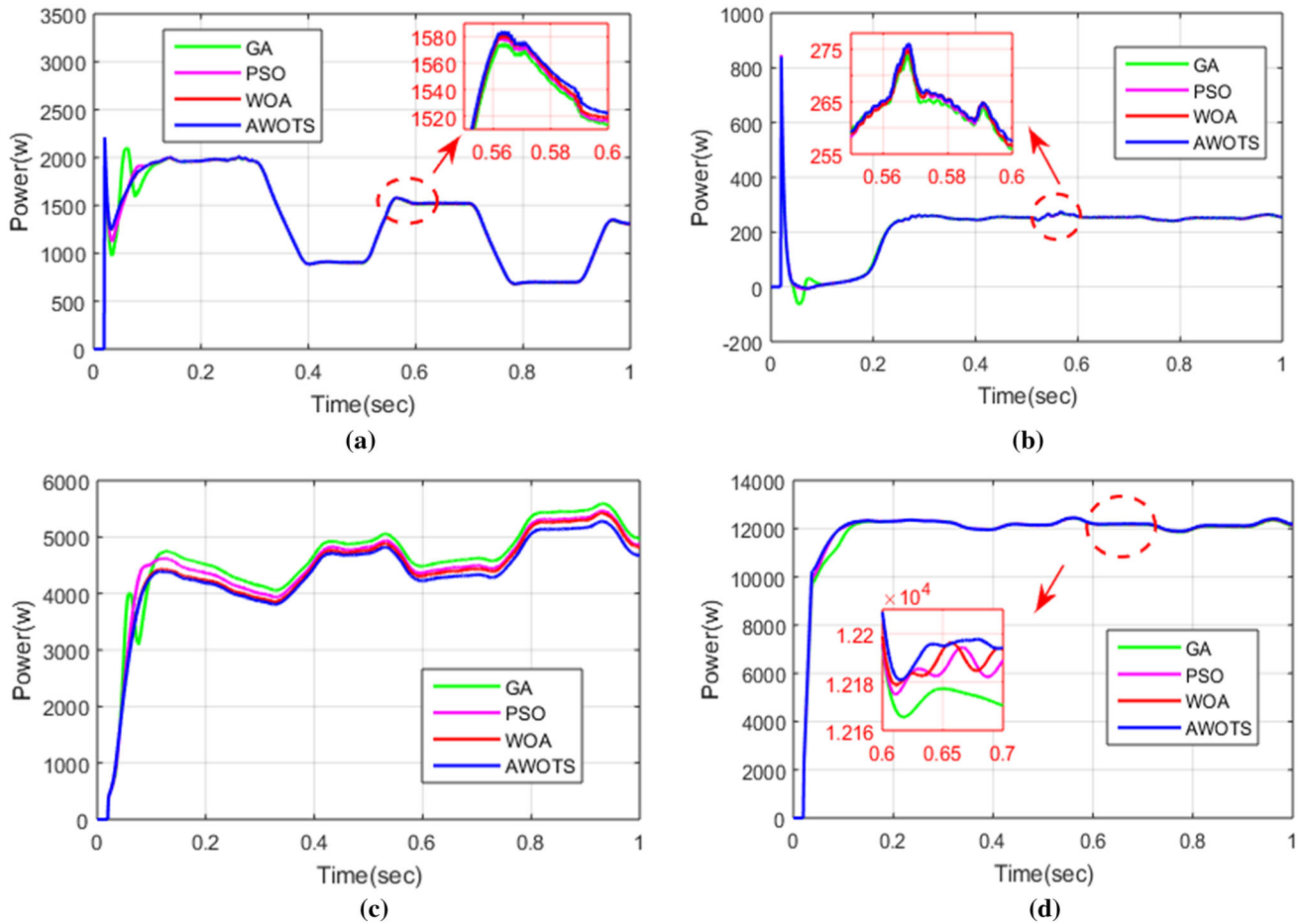


Fig. 11 Individual power comparison using AWO-ANFIS: **a** PV power, **b** wind power, **c** battery power, **d** load power

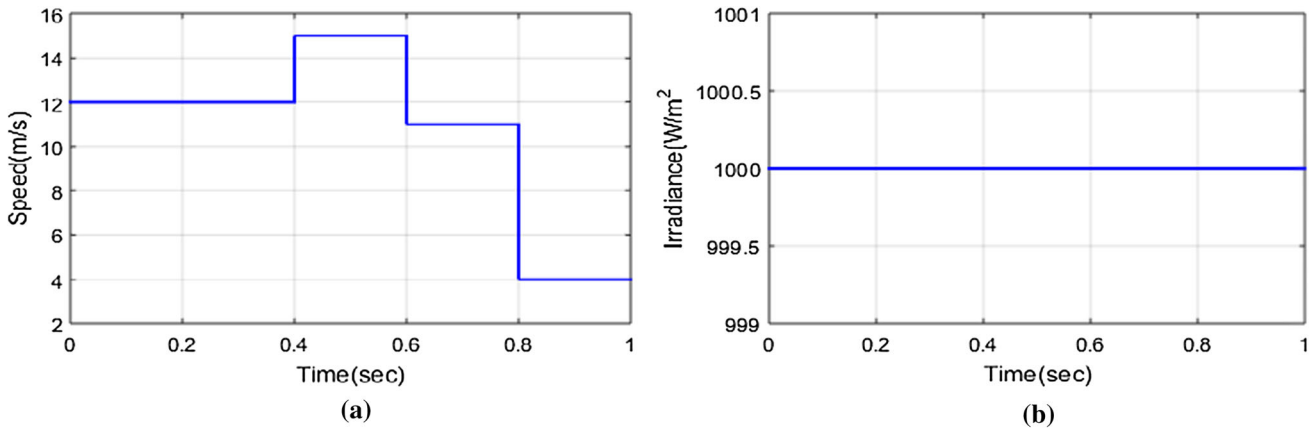


Fig. 12 Variation of wind speed under constant irradiance: **a** wind speed, **b** irradiance

**Case 2: Variation of wind speed under constant irradiance**

In this section, case study 2 delineated the variation of PV power under constant irradiance which is clearly illustrated in Fig. 12. Here, Fig. 12a illustrates the variation of wind speed and Fig. 12b illustrates the constant

irradiance. Learning from this figure, the irradiance and the wind speed are plotted between the time intervals 0 s and 1 s.

Figure 13 illustrates the performance of the proposed method under constant irradiance which has been including the current, voltage and power of the proposed PV, wind and the battery system. Here, Fig. 13a, d, g shows the



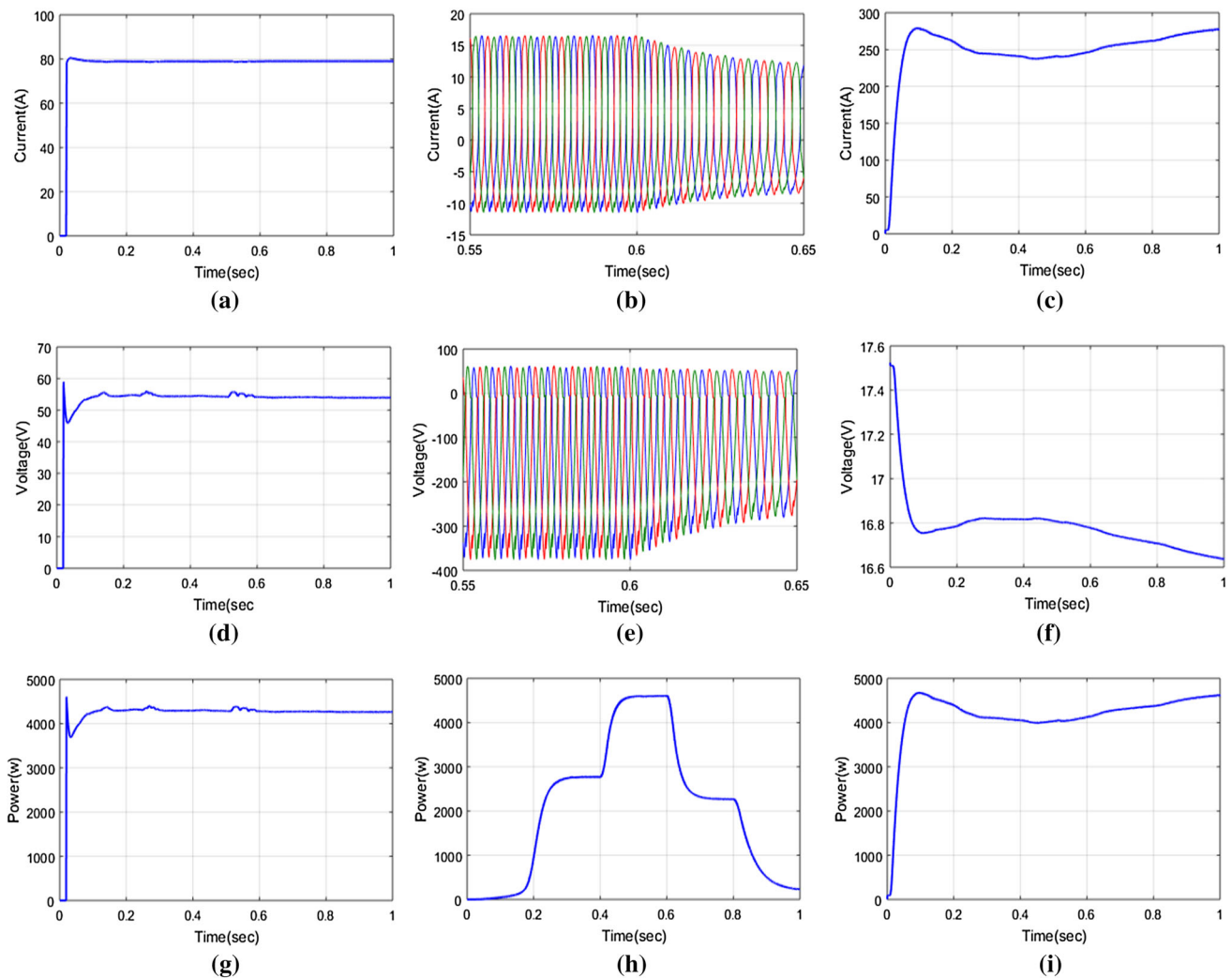


**Fig. 13** Performance under variation of wind speed: **a** PV current, **b** wind current, **c** battery current, **d** PV voltage, **e** wind voltage, **f** battery voltage, **g** PV power, **h** wind power and **i** battery power

current, voltage and power of the PV which has been plotted between the time intervals 0 and 1 s. The maximum value of the current, voltage and power of PV is 80A, 60 V and 4800 W, respectively. Likewise, the current, voltage and power of the wind are illustrated in Fig. 13b, e, h which have been plotted between the time intervals 0.2 and 0.8 s, 0.2 and 0.82 s and 0 and 1 s, respectively.

The maximum value of the current, voltage and power of the wind is 16A, 70 V and 4500 W, respectively. Similarly, the current, voltage and power of the battery are illustrated in Fig. 13c, g, i which have been plotted between the time intervals 0 and 1 s. The maximum value of the current, voltage and power of the battery is 280A, 17.52 V and 4600 W, respectively.

The performance of the dynamic response of the current, voltage and power of the grid, load and inverter is illustrated in Fig. 14. Here, the currents of the grid, load and inverter are illustrated in Fig. 14a–c; these three plots are

varied between the time intervals of 0.1 and 1 s. The maximum values of the current in the grid and load are 3 A, 190 A and 420 A, respectively. The voltage signals of the grid, load and inverter are illustrated in Fig. 14d–f; these three voltage signals are varied between the time intervals of 0.1 and 1 s. The maximum values of the voltage in the grid and load are 700 V, 750 V and 10 V, respectively. The power signals of the grid, load and inverter are illustrated in Fig. 14g–i; these three power signals are varied between the time intervals of 0 and 1 s. The maximum values of the power in the grid, load and inverter are 3000 W, 12000 W and 6000 W, respectively.

Figure 15 shows the performance of the current, voltage and power of the PV, wind and battery by using the AWO-ANFIS control scheme. The current signals of the PV, wind and battery are delineated in Fig. 15a–c. In these three plots, the signal is plotted between the instants of 0 and 1 s. The maximum values of the current in the PV, wind and

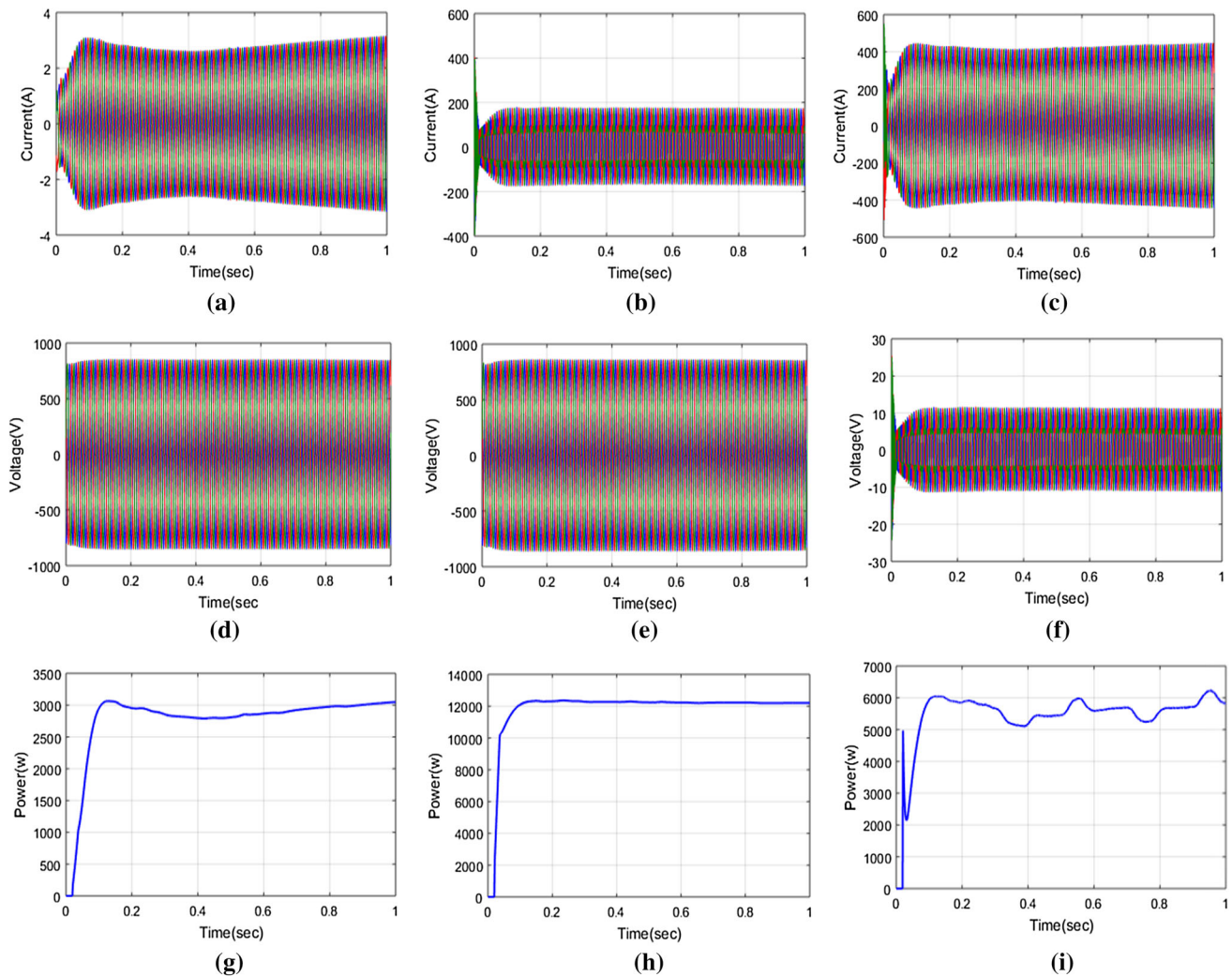


**Fig. 14** Performance of the proposed technique under variation of wind speed: **a** grid current, **b** load current, **c** inverter current, **d** grid voltage, **e** load voltage, **f** inverter voltage **g** grid power, **h** load power and **i** inverter power

battery are 135 A,  $9.99 \times 10^4$  A and 275 A, respectively. Likewise, the voltage signals of the PV, wind and battery are delineated in Fig. 15d–f. In these three plots, the signal is plotted between the instants of 0 and 1 s. The maximum values of the voltage in the PV, wind and battery are 17.5 V, 17 V and 17.8 V, respectively. Similarly, the power signals of the PV, wind and battery are delineated in Fig. 15g–i. In these three plots, the signal is plotted between the instants of 0 and 1 s. The maximum values of the current in the PV, wind and battery are 2400 W, 4.4 W and 4400 W, respectively.

The power comparison of the PV, wind, battery and load are clearly depicted in Fig. 16. Here, the power of the proposed technique is maintained by using AWO-ANFIS control scheme, and also, the performance of the proposed method is compared with that of the GA, PSO and WOA approach. The individual power of PV is illustrated in Fig. 16a; here, the proposed AWO-ANFIS approach has

high power when compared with the existing methods during the time intervals of 0.5 to 0.7 s. The maximum power value of the proposed scheme is 1999 W. In the remaining instants, the power value of all the techniques is similar. The individual power of wind is illustrated in Fig. 16b; here, the proposed AWO-ANFIS approach has high power during the time intervals of 0.5 to 0.6 s. The maximum power value of the proposed scheme is 360 W. The individual power of the battery is illustrated in Fig. 16c; here, the proposed AWO-ANFIS approach has high power during the time intervals of 0.2 to 1 s; here, the maximum power value in the battery is 4500 W. The power of the load is illustrated in Fig. 16d.

### Case 3: Load variation under constant irradiance and wind speed

Case 3 shows the load variation of current, voltage and power under constant irradiance and wind speed which are

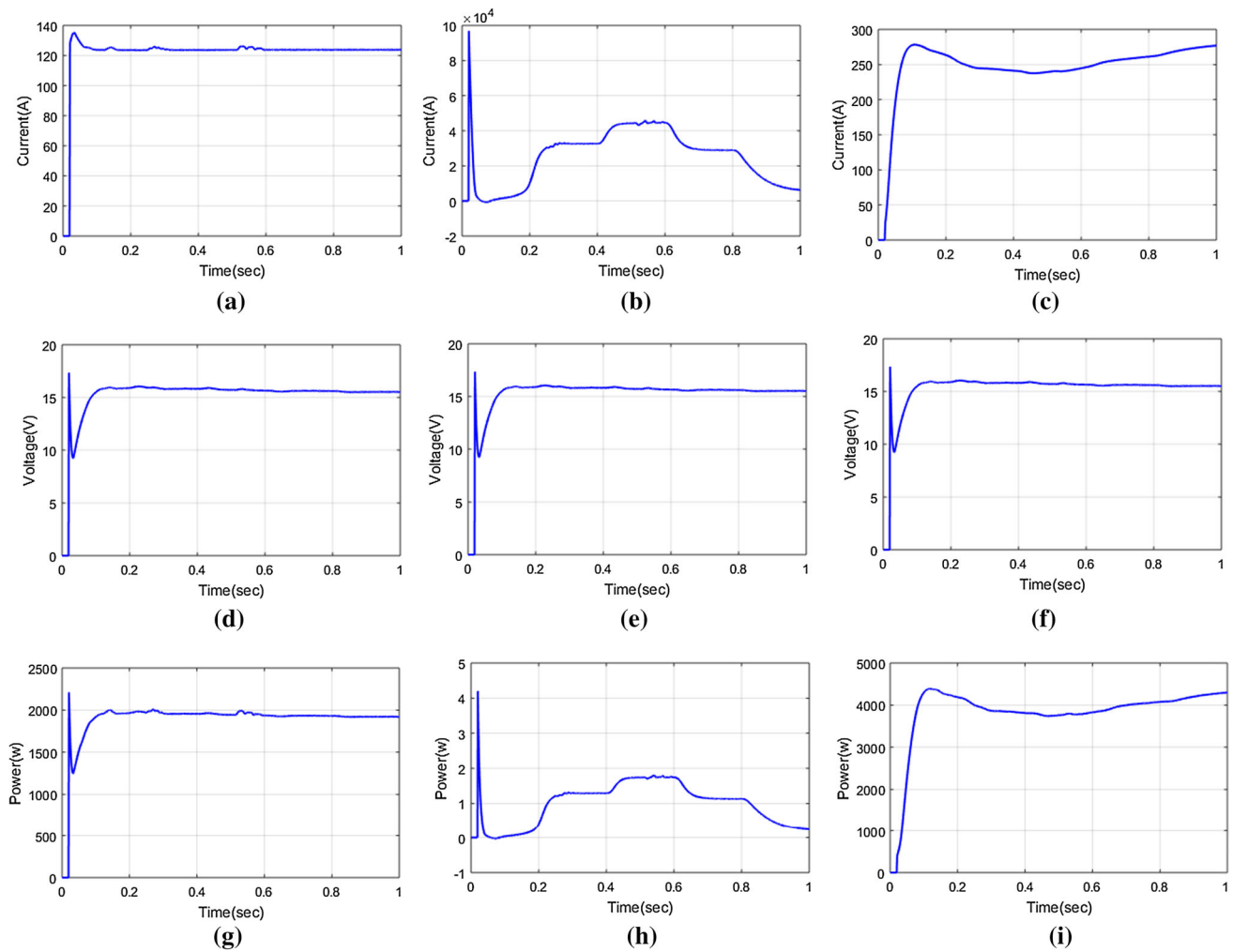


**Fig. 15** Performance of the converter using AWO-ANFIS: **a** PV current, **b** wind current, **c** battery current, **d** PV voltage, **e** wind voltage, **f** battery voltage, **g** PV power, **h** wind power and **i** battery power

clearly depicted in Fig. 17. Here, Fig. 17a–c illustrates the current, voltage and power of the load and Fig. 17d, e illustrates the constant irradiance and wind speed. At the time of constant irradiance and wind speed, the maximum values of the load current, voltage and power are 200A, 600 V and 12000 W, respectively. After reaching the maximum value, the current, voltage and power of the load are going constantly till the end of the operation.

#### 4.1 Comparative analysis

Table 1 includes a classification of the comparative measures for optimization algorithm (Beiranvand et al. 2017). The best function value of the proposed method is illustrated in Fig. 18. This figure includes the function value of the four methods such as GA, PSO, WOA and the proposed AWO-ANFIS. In this plot, all the four methods are starts well, but after some function evaluation, the value is decreased. Initially, the method GA starts well and it is

decreased about 300 function evaluations, while the method PSO shows a steady decrease for about 800 function evaluations. The method WOA decreased after 300 function evaluation. In this plot, the proposed method has the best function value.

The computational accuracy profile is illustrated in Fig. 19. In this plot, the proposed AWO-ANFIS approach has a better accuracy than the existing approaches. The proposed method has greater than 90% of accuracy than the existing method. The statistical analyses of the various approaches are illustrated in Table 2 which includes the mean, median and the standard deviation. The computational time of the proposed and the existing approaches is illustrated in Table 3. The efficiency comparison of power sources under three cases of the proposed and existing techniques is tabulated in Table 4. Table 4 clearly explains the proposed technique efficacy in all the cases with optimal efficiency results. The efficiency is the energy output, divided by the energy input and expressed as a percentage.

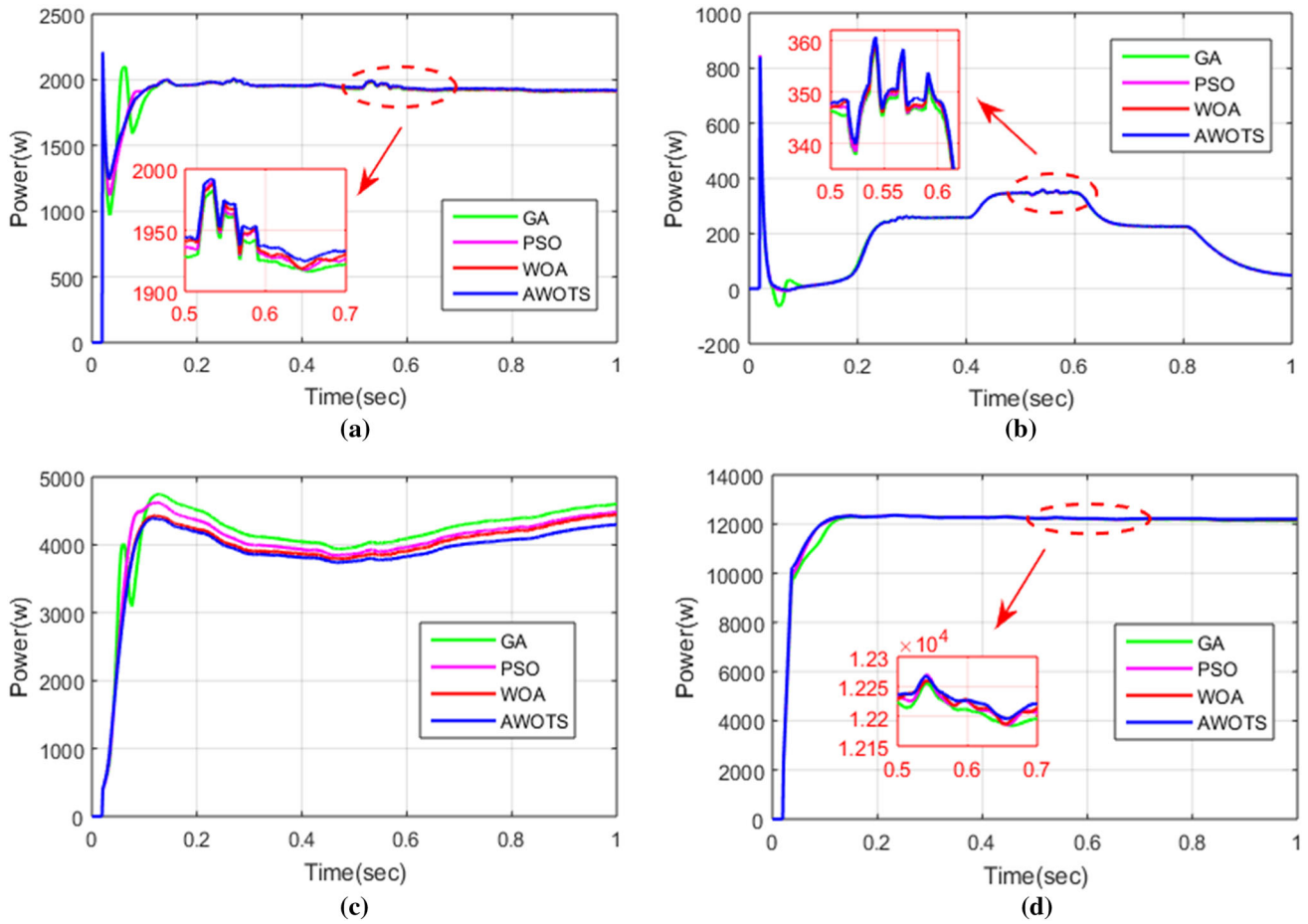


Fig. 16 Individual power comparison using AWO-ANFIS: a PV power, b wind power, c battery power, d load power

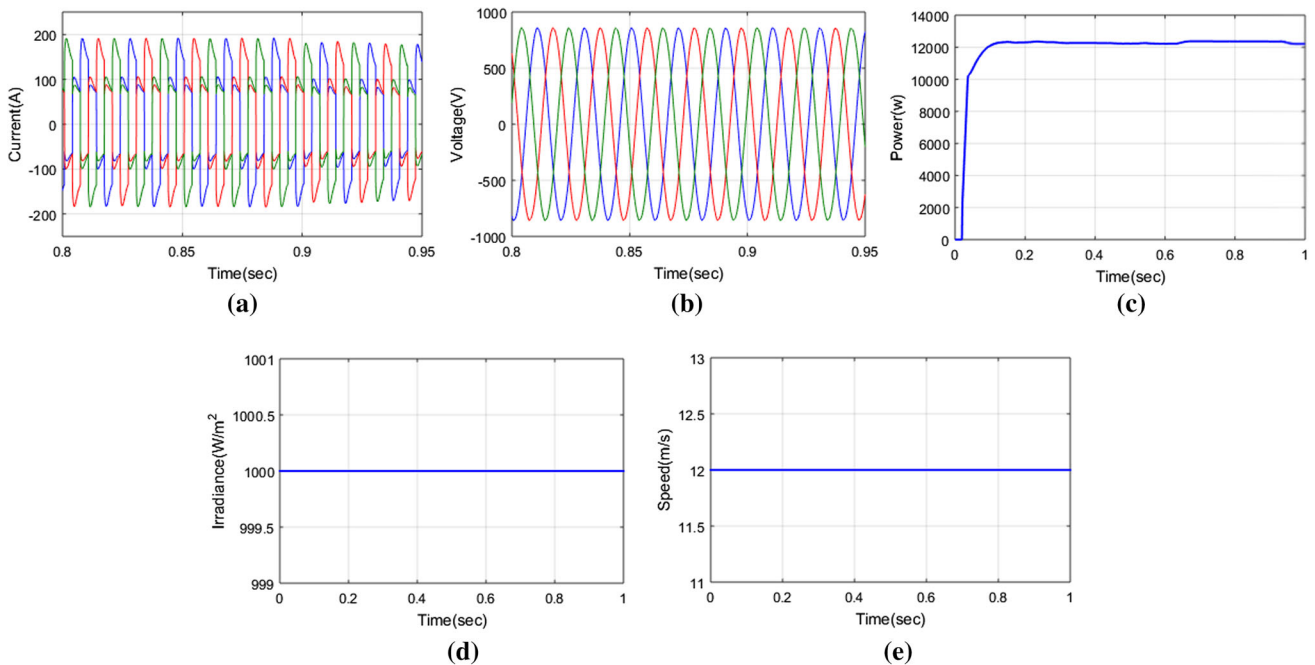


Fig. 17 Performance of load under constant irradiance and wind speed of a load current, b load voltage, c load power, d irradiance and i wind speed

**Table 1** Comparative analysis

Performance category	Example criteria
Efficiency	1. Number of fundamental evaluations 2. Running time 3. Memory usage
Reliability	1. Success rate 2. Number of constraint violations 3. Percentage of global solutions found
Quality of solution	1. Fixed-cost solution result 2. Fixed-target solve time 3. Computational accuracy

At last, it is concluded that the proposed technique is efficient in all the cases by means of reduction in errors and statistical measures. The proposed method gives optimal results when compared with other existing techniques.

### 5 Conclusions

In this dissertation, based on multi-objective optimization, a high-performance AWO-ANFIS control scheme is proposed. The initial-level control scheme describes the optimal dataset generation of the control signal for the offline way based on the power variation between the source side and the load side to achieve minimum power loss. The second-level control scheme predicted the optimal signal for the online way, and also, the control procedure is lead in less execution time. This control scheme takes MG minimum error as an objective to determine the optimal utilization of interconnected RES of MGs. To solve the proposed model, a hybrid method of AWO-ANFIS control scheme is applied. The simulation results show that when MGs are integrated with AWO-ANFIS control scheme, the

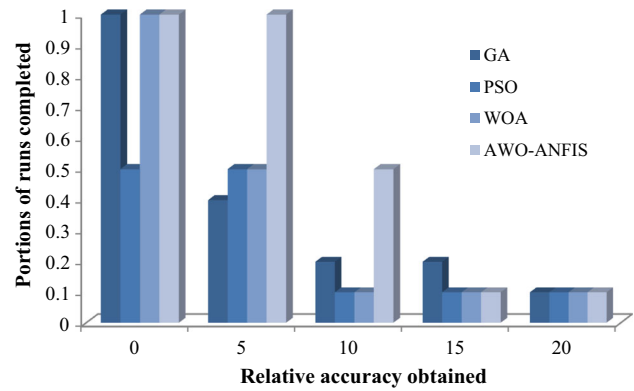


**Fig. 19** Accuracy profile

**Table 2** Statistical analysis of various techniques

Methods	Mean	Median	SD
AWO-ANFIS	2.0092	2.2895	0.0070
GA	2.1780	2.3284	0.0087
PSO	2.2832	2.3836	0.0097
WOA	2.3467	2.4468	0.0121

**Table 3** Computation time using various trails

Trails	Computation time (s)			
	AWO-ANFIS	GA	PSO	WOA
100	5600	5850	5900	6000
250	14,000	14,420	14,865	15,230
500	28,000	28,355	28,843	30,170
1000	56,000	56,420	56,760	56,900

whole MG systems are optimized in better way. The cost and the error of the system are reduced by this model. In the simulation section, the existing techniques such as GA, PSO and WOA are compared with the proposed AWO-

**Fig. 18** Convergence plot

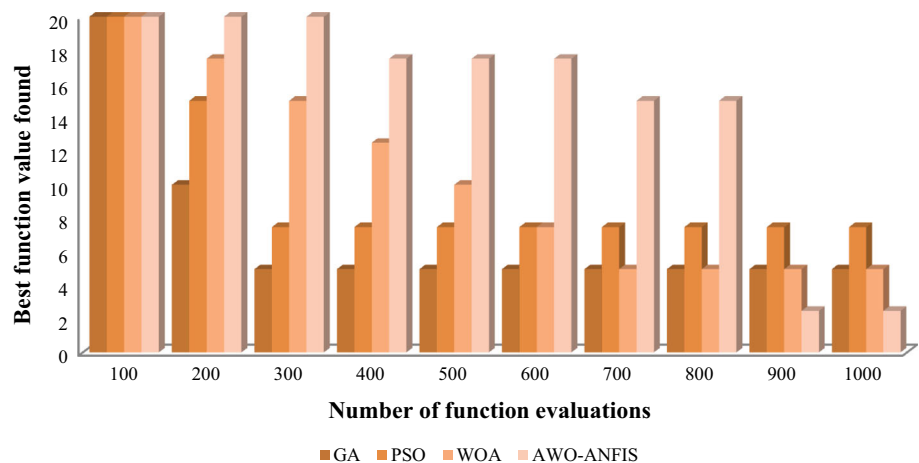




**Table 4** Efficiency comparison of HRES power under all cases

Solution techniques	Case 1			Case 2			Case 3		
	Sources			Sources			Sources		
	PV	WT	Battery	PV	WT	Battery	PV	WT	Battery
<i>Efficiency of HRES power under all cases (%)</i>									
GA	79.265	66.289	79.951	72.57	65.65	44.16	55.348	77.36	59.612
PSO	82.237	65.236	78.92	43.59	59.23	71.58	77.771	65.21	54.789
WOA	86.182	87.065	77.357	76.98	87.67	78.923	77.515	85.23	82.369
Proposed technique	98.935	95.35	97.087	92.36	97.51	99.73	89.645	88.26	91.0213

ANFIS approach for the performance analysis by using the three types of case studies (i) variation of irradiance, (ii) variation of wind speed and (iii) variation of load. For all the cases, the proposed technique exhibits better performance in terms of current, voltage and power signal. The proposed method is implemented by using MATLAB/Simulink working platform. This paper provides a positive reference for the application and expansion of future optimization-based MG systems.

**Acknowledgements** No funding has been received.

## Compliance with ethical standards

**Conflict of interest** The authors declare that they have no conflict of interest.

**Ethical approval** This article does not contain any studies with human participants performed by any of the authors.

## References

- Abualigah LMQ (2019) Feature selection and enhanced krill herd algorithm for text document clustering. *Studies in computational intelligence*. Springer, Berlin
- Abualigah LMQ, Hanandeh ES (2015) Applying genetic algorithms to information retrieval using vector space model. *Int J Comput Sci Eng Appl* 5(1):19. <https://doi.org/10.5121/ijcsea.2015.5102>
- Abualigah LM, Khader AT (2017) Unsupervised text feature selection technique based on hybrid particle swarm optimization algorithm with genetic operators for the text clustering. *J Supercomput* 73(11):4773–4795. <https://doi.org/10.1007/s11227-017-2046-2>
- Abualigah LM, Khader AT, Hanandeh ES (2017) A new feature selection method to improve the document clustering using particle swarm optimization algorithm. *J Comput Sci* 25:456–466. <https://doi.org/10.1016/j.jocs.2017.07.018>
- Abualigah LM, Khader AT, Hanandeh ES (2018a) Hybrid clustering analysis using improved krill herd algorithm. *Appl Intell* 48(11):4047–4071. <https://doi.org/10.1007/s10489-018-1190-6>
- Abualigah LM, Khader AT, Hanandeh ES (2018b) A combination of objective functions and hybrid krill herd algorithm for text document clustering analysis. *Eng Appl Artif Intell* 73:111–125. <https://doi.org/10.1016/j.engappai.2018.05.003>
- Aljarah I, Faris H, Mirjalili S (2016) Optimizing connection weights in neural networks using the whale optimization algorithm. *Soft Comput* 22:1–15. <https://doi.org/10.1007/s00500-016-2442-1>
- Almada J, Leão R, Sampaio R, Barroso G (2016) A centralized and heuristic approach for energy management of an AC microgrid. *Renew Sustain Energy Rev* 60:1396–1404. <https://doi.org/10.1016/j.rser.2016.03.002>
- Ambia M, Al-Durra A, Caruana C, Muyeen S (2014) Power management of hybrid micro-grid system by a generic centralized supervisory control scheme. *Sustain Energy Technol Assess* 8:57–65. <https://doi.org/10.1016/j.seta.2014.07.003>
- Amin F, Fahmi A (2019) Human immunodeficiency virus (HIV) infection model based on triangular neutrosophic cubic hesitant fuzzy number. *Int J Biomath*. <https://doi.org/10.1142/S1793524519500554>
- Amin F, Fahmi A, Abdullah S, Ali A, Ahmad R, Ghani F (2017) Triangular cubic linguistic hesitant fuzzy aggregation operators and their application in group decision making. *J Intell Fuzzy Syst* 34:2401–2416. <https://doi.org/10.3233/JIFS-171567>
- Amirtharaj S, Premalatha L, Gopinath D (2019) Optimal utilization of renewable energy sources in MG connected system with integrated converters: an AGONN approach. *Analog Integr Circ Sig Process* 101(3):513–532. <https://doi.org/10.1007/s10470-019-01452-8>
- Angalaeswari S, Swathika OG, Ananthkrishnan V, Daya JF, Jamuna K (2017) Efficient power management of grid operated micro-grid using fuzzy logic controller (FLC). *Energy Procedia* 117:268–274. <https://doi.org/10.1016/j.egypro.2017.05.131>
- Aujla G, Kumar N (2018) SDN-based energy management scheme for sustainability of data centers: an analysis on renewable energy sources and electric vehicles participation. *J Parallel Distrib Comput* 117:228–245. <https://doi.org/10.1016/j.jpdc.2017.07.002>
- Basir Khan M, Jidin R, Pasupuleti J (2016) Multi-agent based distributed control architecture for microgrid energy management and optimization. *Energy Convers Manag* 112:288–307. <https://doi.org/10.1016/j.enconman.2016.01.011>
- Beiranvand V, Hare W, Lucet Y (2017) Best practices for comparing optimization algorithms. *Optim Eng* 18(4):815–848. <https://doi.org/10.1007/s11081-017-9366-1>
- Bruni G, Cordiner S, Mulone V, Sinisi V, Spagnolo F (2016) Energy management in a domestic microgrid by means of model predictive controllers. *Energy* 108:119–131. <https://doi.org/10.1016/j.energy.2015.08.004>
- Duan D, Ling X, Wu X, Zhong B (2015) Reconfiguration of distribution network for loss reduction and reliability improvement based on an enhanced genetic algorithm. *Int J Electr Power Energy Syst* 64:88–95. <https://doi.org/10.1016/j.ijepes.2014.07.036>
- Fahmi A, Abdullah S, Amin F, Ali A (2017a) precursor selection for sol-gel synthesis of titanium carbide nanopowders by a new cubic fuzzy multi-attribute group decision-making model. *J Intell Syst*. <https://doi.org/10.1515/jisys-2017-0083>
- Fahmi A, Abdullah S, Amin F, Aslam M, Hussain S (2017b) Trapezoidal linguistic cubic fuzzy TOPSIS method and



- application in a group decision making program. *J Intell Syst*. <https://doi.org/10.1515/jisys-2017-0560>
- Fahmi A, Abdullah S, Amin F, Siddiqui N, Ali A (2017c) Aggregation operators on triangular cubic fuzzy numbers and its application to multi-criteria decision making problems. *J Intell Fuzzy Syst* 33:3323–3337. <https://doi.org/10.3233/JIFS-162007>
- Fahmi A, Abdullah S, Amin F, Ali A (2018a) Weighted average rating (war) method for solving group decision making problem using triangular cubic fuzzy hybrid aggregation (Tcfha). *Punjab Univ J Math* 50(1):23–34
- Fahmi A, Abdullah S, Amin F, Ali A, Ahmad Khan W (2018b) Some geometric operators with triangular cubic linguistic hesitant fuzzy number and their application in group decision-making. *J Intell Fuzzy Syst*. <https://doi.org/10.3233/JIFS-18125>
- Fahmi A, Abdullah S, Amin F, Khan MS (2018c) Trapezoidal cubic fuzzy number einstein hybrid weighted averaging operators and its application to decision making. *Soft Comput* 23(14):5753–5783. <https://doi.org/10.1007/s00500-018-3242-6>
- Fahmi A, Amin F, Abdullah S, Ali A (2018d) Cubic fuzzy Einstein aggregation operators and its application to decision making. *Int J Syst Sci* 49(11):2385–2397. <https://doi.org/10.1080/00207721.2018.1503356>
- Fahmi A, Amin F, Smarandache F, Khan M, Hassan N (2018e) Triangular cubic hesitant fuzzy einstein hybrid weighted averaging operator and its application to decision making. *Symmetry* 10(11):658. <https://doi.org/10.3390/sym10110658>
- Fahmi A, Abdullah S, Amin F (2019a) Cubic uncertain linguistic powered Einstein aggregation operators and their application to multi-attribute group decision making. *Math Sci*. <https://doi.org/10.1007/s40096-019-0285-5>
- Fahmi A, Abdullah S, Amin F, Ali A, Ahmad R, Shakeel M (2019b) Trapezoidal cubic hesitant fuzzy aggregation operators and their application in group decision-making. *J Intell Fuzzy Syst* 36(4):3619–3635. <https://doi.org/10.3233/JIFS-181703>
- Fahmi A, Amin F, Khan M, Smarandache F (2019c) Group decision making based on triangular neutrosophic cubic fuzzy einstein hybrid weighted averaging operators. *Symmetry* 11(2):180. <https://doi.org/10.3390/sym11020180>
- Goroohi Sardou I, Zare M, Azad-Farsani E (2018) Robust energy management of a microgrid with photovoltaic inverters in VAR compensation mode. *Int J Electr Power Energy Syst* 98:118–132. <https://doi.org/10.1016/j.ijepes.2017.11.037>
- Indragandhi V, Logesh R, Subramaniaswamy V et al (2018) Multi-objective optimization and energy management in renewable based AC/DC microgrid. *Comput Electr Eng* 70:179–198. <https://doi.org/10.1016/j.compeleceng.2018.01.023>
- Javaid N, Naseem M, Rasheed MB, Mahmood D, Khan SA, Alrajeh N, Iqbal Z (2017) A new heuristically optimized home energy management controller for smart grid. *Sustain Cities Soc* 34:211–227. <https://doi.org/10.1016/j.scs.2017.06.009>
- Jordehi AR, Jasni J, Wahab NA, Kadir MZ, Javadi MS (2015) Enhanced leader PSO (ELPSO): A new algorithm for allocating distributed TCSC's in power systems. *Int J Electr Power Energy Syst* 64:771–784. <https://doi.org/10.1016/j.ijepes.2014.07.058>
- Kaur J, Sood Y, Shrivastava R (2019) Optimal resource utilization in a multi-microgrid network for Tamil Nadu state in India. *IETE J Res* 5:1–11. <https://doi.org/10.1080/03772063.2019.1595182>
- Kaveh A, Ghazaan M (2016) Enhanced whale optimization algorithm for sizing optimization of skeletal structures. *Mech Based Des Struct Mach* 45:345–362. <https://doi.org/10.1080/15397734.2016.1213639>
- Kim K, Cha H, Park S, Lee I (2018) A modified series-capacitor high conversion ratio DC–DC converter eliminating start-up voltage stress problem. *IEEE Trans Power Electron* 33:8–12. <https://doi.org/10.1109/tpe.2017.2705705>
- Mafarja M, Mirjalili S (2017) Hybrid whale optimization algorithm with simulated annealing for feature selection. *Neurocomputing* 260:302–312. <https://doi.org/10.1016/j.neucom.2017.04.053>
- Mirjalili S, Lewis A (2016) The whale optimization algorithm. *Adv Eng Softw* 95:51–67. <https://doi.org/10.1016/j.advengsoft.2016.01.008>
- Mohamed Imran A, Kowsalya M (2014) A new power system reconfiguration scheme for power loss minimization and voltage profile enhancement using Fireworks Algorithm. *Int J Electr Power Energy Syst* 62:312–322. <https://doi.org/10.1016/j.ijepes.2014.04.034>
- Nürnberg A, Nauck D, Kruse R (1999) Neuro-fuzzy control based on the NEFCON-model: recent developments. *Soft Comput Fusion Found Methodol Appl* 2:168–182. <https://doi.org/10.1007/s005000050050>
- Olatomiwa L, Mekhilef S, Ismail M, Moghavvemi M (2016) Energy management strategies in hybrid renewable energy systems: a review. *Renew Sustain Energy Rev* 62:821–835. <https://doi.org/10.1016/j.rser.2016.05.040>
- Oliva D, Abd El Aziz M, Ella Hassanien A (2017) Parameter estimation of photovoltaic cells using an improved chaotic whale optimization algorithm. *Appl Energy* 200:141–154. <https://doi.org/10.1016/j.apenergy.2017.05.029>
- Patrone M, Feroldi D (2017) Passivity-based control design for a grid-connected hybrid generation system integrated with the energy management strategy. *J Process Control*. <https://doi.org/10.1016/j.jprocont.2017.11.012>
- Prince S, Panda K, Kumar V, Panda G (2018) Power quality enhancement in a distribution network using PSO assisted Kalman filter—based shunt active power filter. In: 2018 IEEMA engineer infinite conference (eTechNxt). New Delhi, India, pp 1–6. <https://doi.org/10.1109/etechnxt.2018.8385314>
- Rahim S, Javaid N, Ahmad A, Khan SA, Khan ZA, Alrajeh N, Qasim U (2016) Exploiting heuristic algorithms to efficiently utilize energy management controllers with renewable energy sources. *Energy Build* 129:452–470. <https://doi.org/10.1016/j.enbuild.2016.08.008>
- Roy K, Mandal K, Mandal A (2019) Ant-Lion Optimizer algorithm and recurrent neural network for energy management of micro grid connected system. *Energy* 167:402–416. <https://doi.org/10.1016/j.energy.2018.10.153>
- Sahu P, Hota P, Panda S (2018) Power system stability enhancement by fractional order multi input SSSC based controller employing whale optimization algorithm. *J Electr Syst Inf Technol*. <https://doi.org/10.1016/j.jesit.2018.02.008>
- Selvara V (2017) Adaptive neuro fuzzy inference systems based clustering approach for wireless sensor networks. *Int J Eng Comput Sci*. <https://doi.org/10.18535/ijecs/v6i11.11>
- Wu X, Hu X, Moura S et al (2016) Stochastic control of smart home energy management with plug-in electric vehicle battery energy storage and photovoltaic array. *J Power Sources* 333:203–212. <https://doi.org/10.1016/j.jpowsour.2016.09.157>
- Yadegaridehkordi E, Nilashi M, Nasir M, Ibrahim O (2018) Predicting determinants of hotel success and development using Structural Equation Modelling (SEM)-ANFIS method. *Tour Manag* 66:364–386. <https://doi.org/10.1016/j.tourman.2017.11.012>
- Zhang J, Huang L, Shu J, Wang H, Ding J (2017) Energy management of PV-diesel-battery hybrid power system for island stand-alone micro-grid. *Energy Procedia* 105:2201–2206. <https://doi.org/10.1016/j.egypro.2017.03.622>